



**Aggregation Induced Emission from a new Naphthyridine-ethynyl-Gold(I) Complex as a potential tool for sensing Guanosine Nucleotides in Aqueous Media**

Journal:	<i>Dalton Transactions</i>
Manuscript ID	DT-ART-10-2019-004162.R1
Article Type:	Paper
Date Submitted by the Author:	n/a
Complete List of Authors:	Moro, Artur; Universidade Nova de Lisboa, REQUIMTE, Dep. Química Avó, João; Universidade de Lisboa Instituto Superior Tecnico, CQFM-IN and IBB-Institute for Bioengineering and Biosciences Malfois, Marc; ALBA Synchrotron Light Laboratory (CELLS)., Carrer de la Llum 2-26. 08290 Cerdanyola del Vallès Zaccaria, Francesco; Vrije Universiteit Amsterdam, Fonseca Guerra, Célia; VU University, Theoretical Chemistry Caparrós, Francisco Javier; Universitat de Barcelona, Inorganic and Organic Departament Rodriguez, Laura; Universitat de Barcelona, Inorganic and Organic Departament Lima, J. C.; REQUIMTE, Chemistry

# Dalton Transactions

An international journal of inorganic chemistry

## Guidelines for Referees

Thank you very much for agreeing to review this manuscript for [Dalton Transactions](#).



*Dalton Transactions* is a journal for all areas of inorganic chemistry, which encompasses the organometallic, bioinorganic and materials chemistry of the elements, with applications including synthesis, catalysis, energy conversion/storage, electrical devices and medicine.

*Dalton Transactions* welcomes high-quality, original submissions in all of these areas and more, where the advancement of knowledge in inorganic chemistry is significant.

*Dalton Transactions*' Impact Factor is **4.052** (2018 Journal Citation Reports®)

---

*The following manuscript has been submitted for consideration as a*

## **PAPER**

---

*Dalton Transactions* wishes to encourage high quality articles reporting exciting new developments in inorganic chemistry.

For an article to be accepted, it must report new, high-quality research and make a significant contribution to the field.

We ask referees to **recommend only the most significant work** for publication in *Dalton Transactions*. When making your recommendation please:

- **Comment on** the originality, importance, impact and scientific reliability of the work
- **Note that routine or incremental** work should not be recommended for publication.
- **Contact the Editor** if there is any conflict of interest, if the work has been previously published or if there is a significant part of the work which you are not able to referee with confidence.

Best regards,

Contact us

**Professor John Arnold**

Editorial Board Chair, *Dalton Transactions*

**Dr Andrew Shore**

Executive Editor, *Dalton Transactions*

Please visit our [reviewer hub](#) for further details of our processes, policies and reviewer responsibilities as well as guidance on how to review, or click the links below.



What to do  
when you  
review



Reviewer  
responsibilities



Process &  
policies

## Supporting Information

### Aggregation Induced Emission from a new Naphthyridine-ethynyl-Gold(I) Complex as a potential tool for sensing Guanosine Nucleotides in Aqueous Media

Artur J. Moro,<sup>a\*</sup> João Avó,<sup>b</sup> Marc Malfois,<sup>c</sup> Francesco Zaccaria,<sup>d</sup> Célia Fonseca Guerra,<sup>d</sup> Francisco J. Caparrós,<sup>e,f</sup> Laura Rodríguez,<sup>e,f</sup> and João Carlos Lima<sup>a</sup>

<sup>a</sup> LAQV-REQUIMTE, Departamento de Química, CQFB, Universidade Nova de Lisboa, Monte de Caparica, Portugal. E-mail:ajm12769@fct.unl.pt

<sup>b</sup>Instituto Superior Técnico, Universidade de Lisboa,

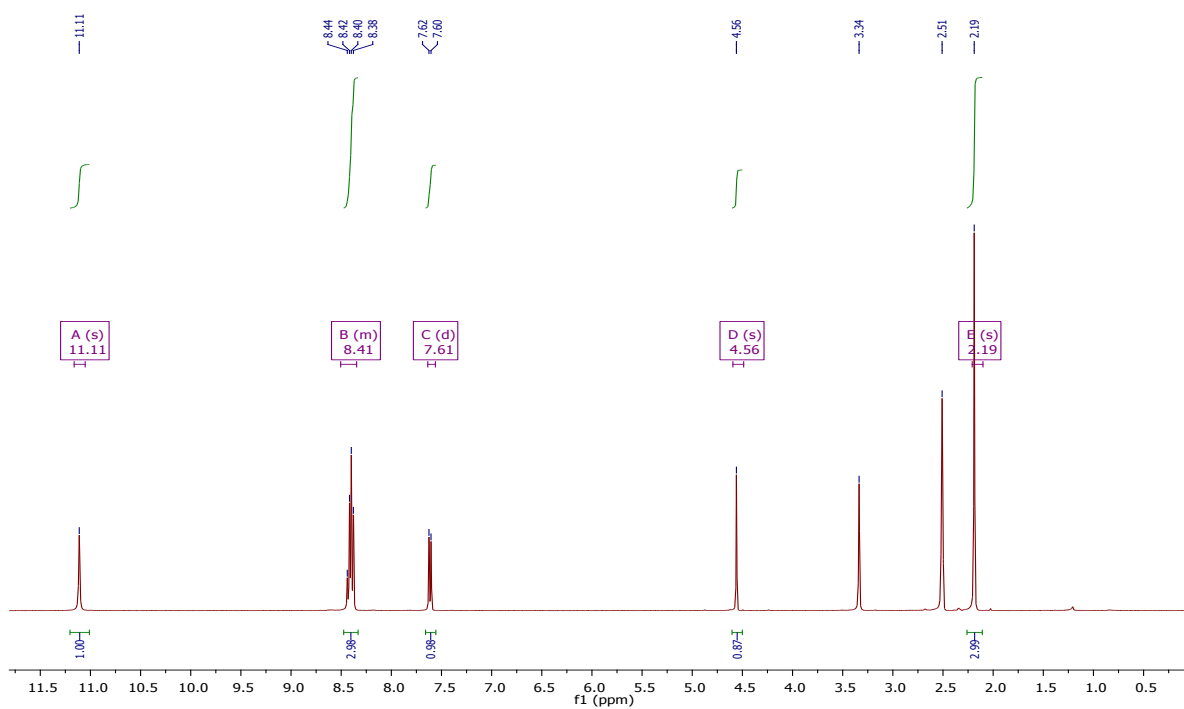
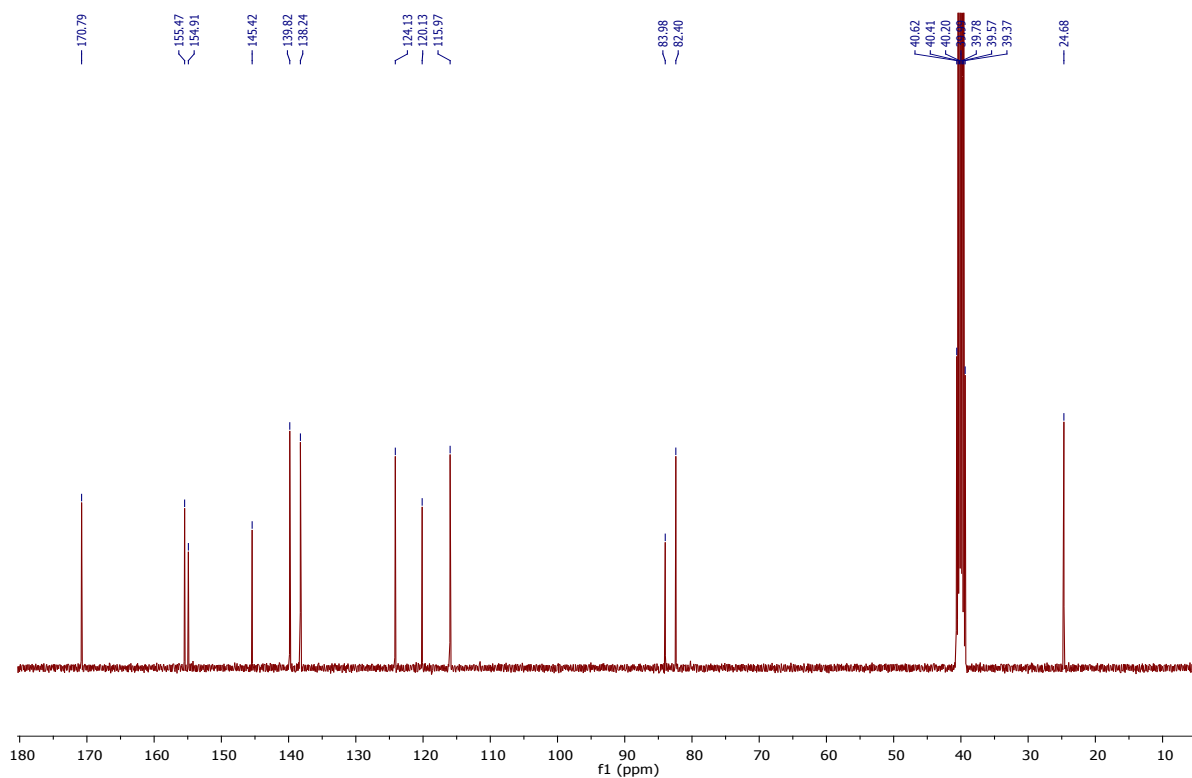
<sup>c</sup>ALBA Synchrotron Light Laboratory (CELLS), Carrer de la Llum 2–26, 08290 Cerdanyola del Vallès, Barcelona, Spain

<sup>d</sup>Department of Theoretical Chemistry, Amsterdam Center for Multiscale Modeling, 1081 HV Amsterdam, The Netherlands

<sup>e</sup>Departament de Química Inorgànica i Orgànica. Secció de Química Inorgànica. Universitat de Barcelona, Martí i Franquès 1-11, 08028 Barcelona, Spain.

<sup>f</sup>Institut de Nanociència i Nanotecnologia (IN<sup>2</sup>UB). Universitat de Barcelona, 08028 Barcelona (Spain)

## NMR Spectra/Data

Figure S1.  $^1\text{H}$  NMR spectrum of **2** in DMSO.Figure S2.  $^{13}\text{C}$  NMR spectrum of **2** in DMSO.

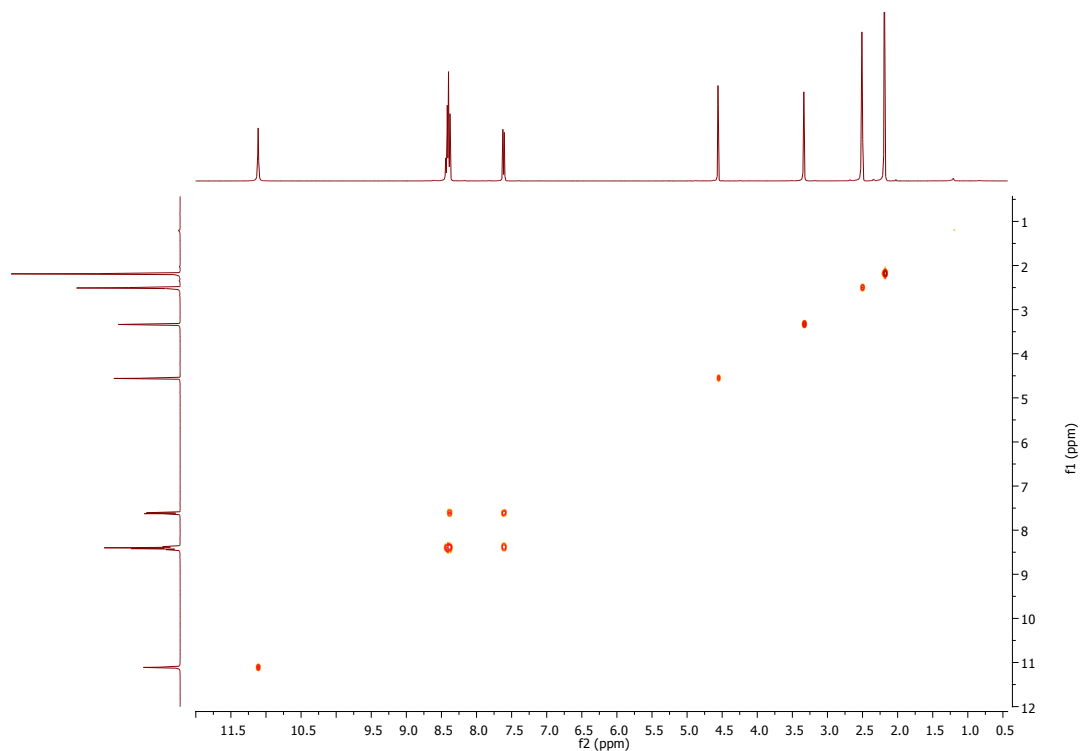


Figure S3.  $^1\text{H}$ - $^1\text{H}$  COSY NMR spectrum of **2** in DMSO.

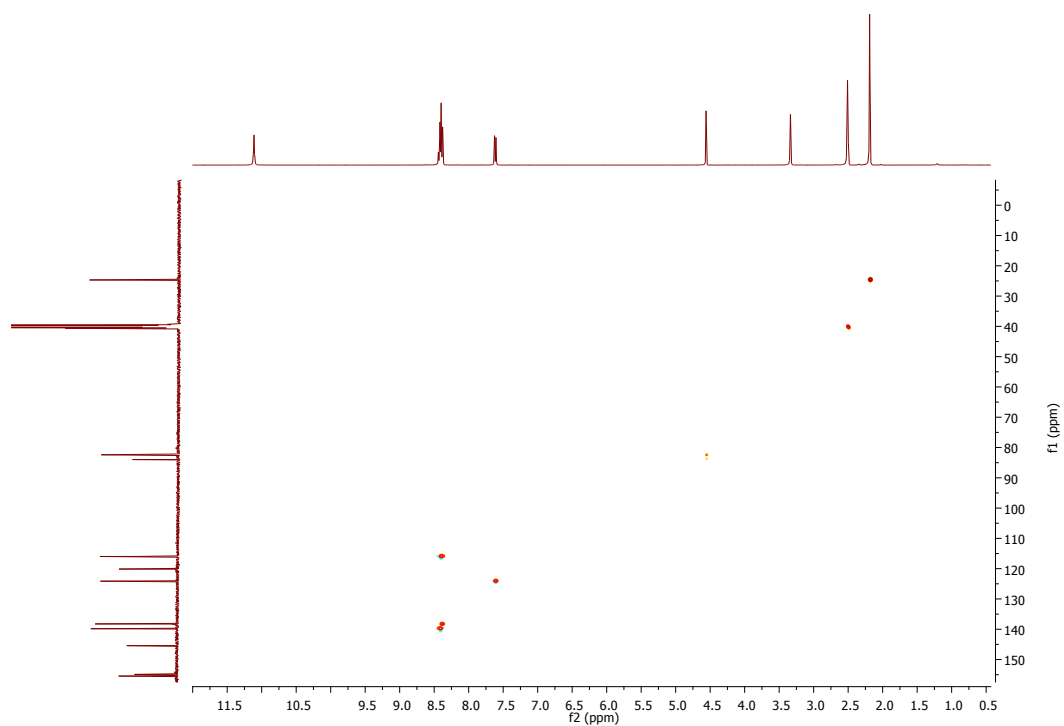
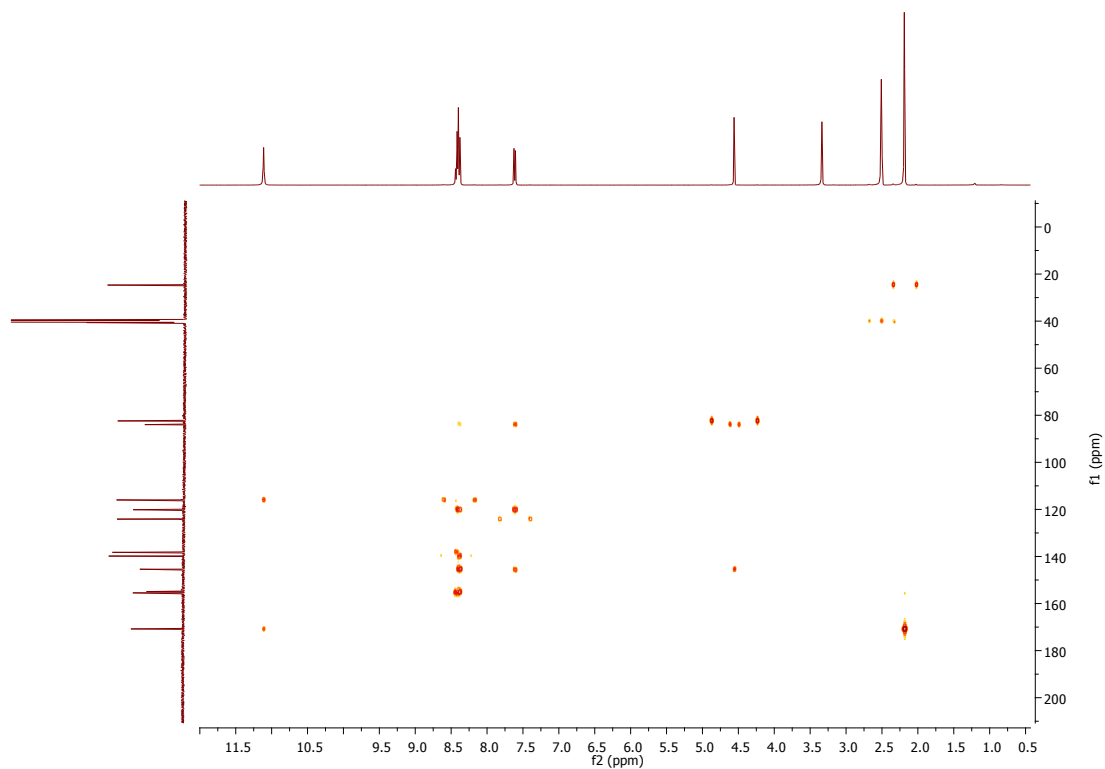
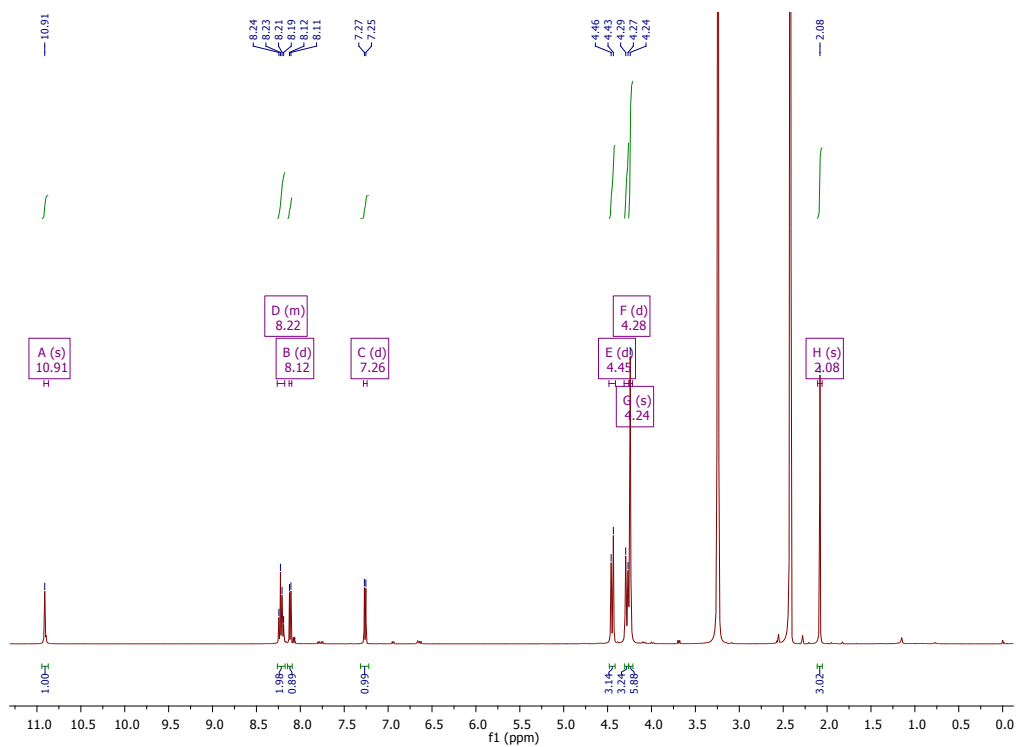
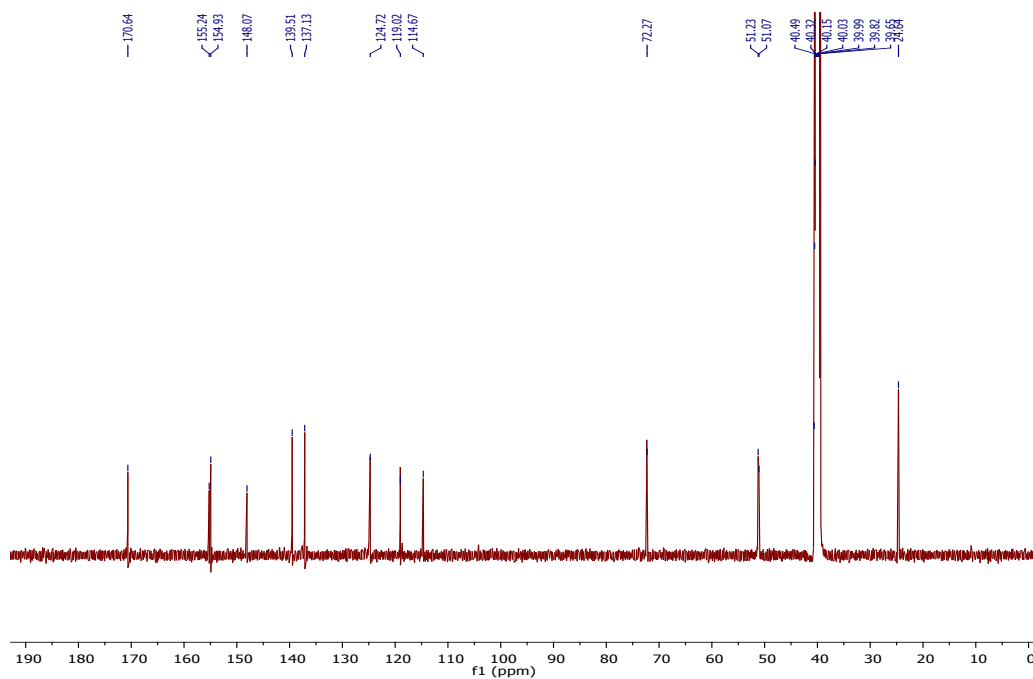


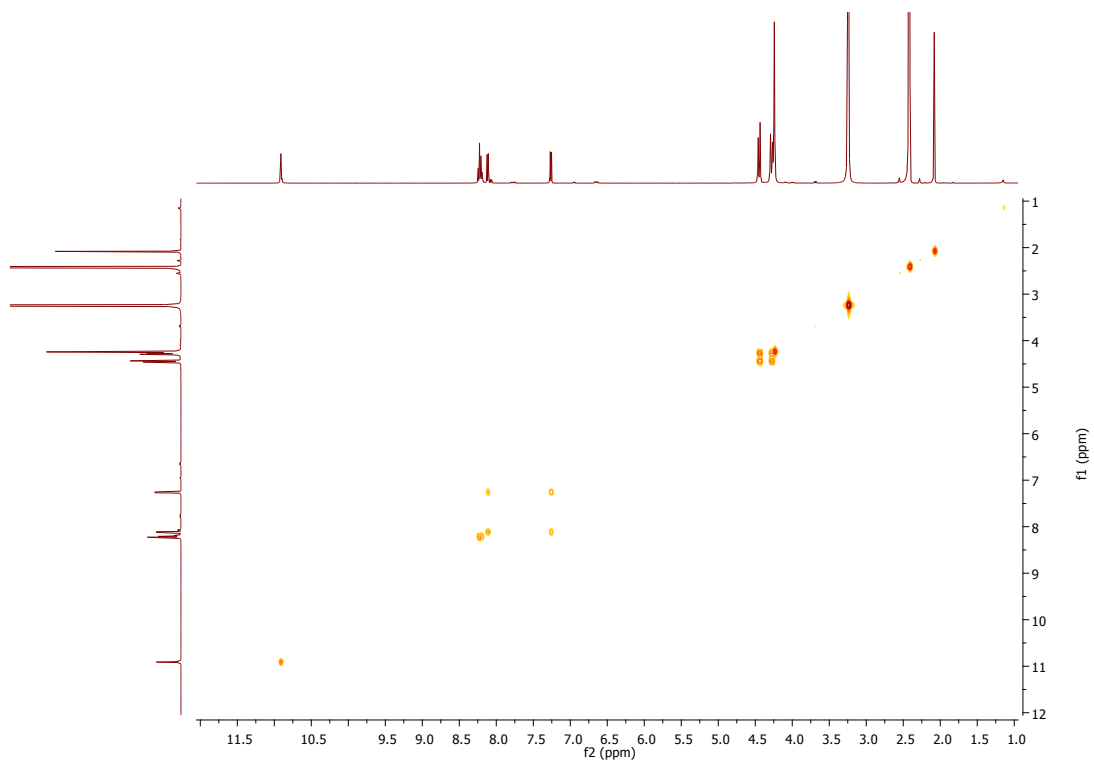
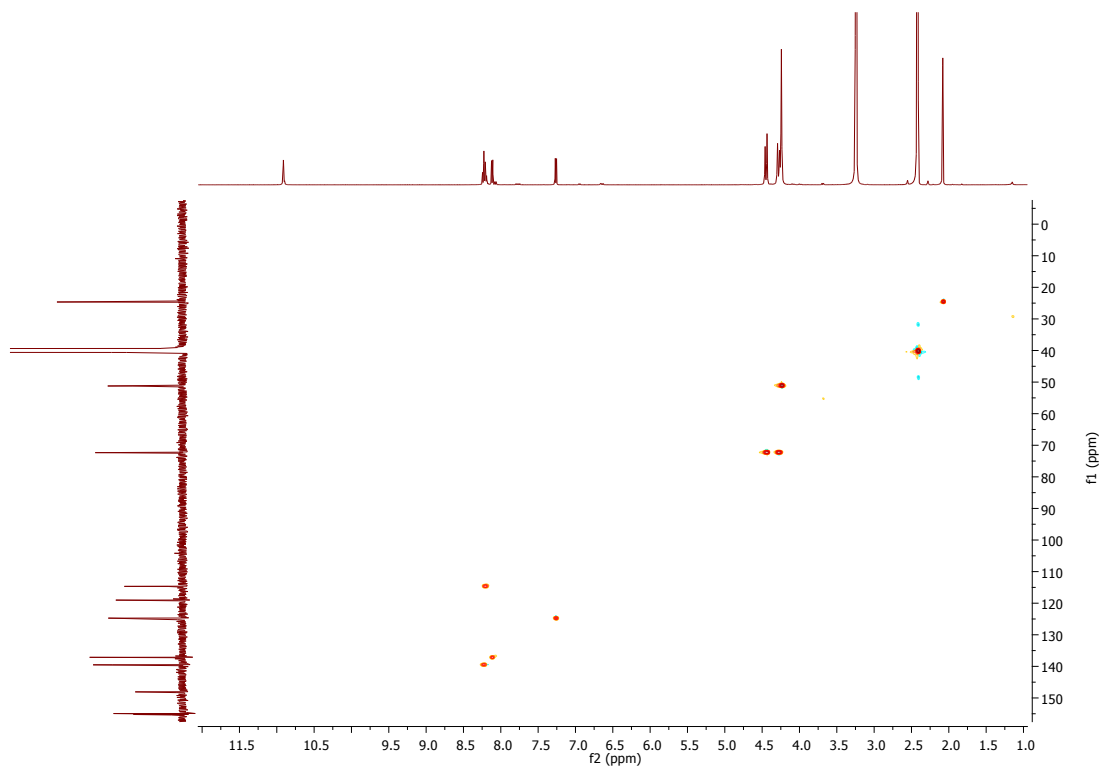
Figure S4.  $^1\text{H}$ - $^{13}\text{C}$  HSQC NMR spectrum of **2** in DMSO.

Figure S5.  $^1\text{H}$ - $^{13}\text{C}$ HMBC NMR spectrum of **2** in DMSO.Table S1. NMR peak assignment for **2**.

Position	$^1\text{H}$	$^{13}\text{C}$
1	-	-
2	-	155.47*
3	8.44-8.38	115.97
4	8.44-8.38	139.82
5	8.44-8.38	138.24
6	7.61	124.13
7	-	145.42
8	-	-
9	-	154.91*
10	-	120.13
11	-	83.98
12	4.56	82.40
13	11.11	-
14	-	170.79
15	2.19	24.68

\*These  $^{13}\text{C}$  signals are too close in chemical shifts for an unequivocal heteronuclear correlation.

Figure S6.  $^1\text{H}$  NMR spectrum of **3** in DMSO.Figure S7.  $^{13}\text{C}$  NMR spectrum of **3** in DMSO.

Figure S8.  $^1\text{H}$ - $^1\text{H}$  COSY NMR spectrum of **3** in DMSO.Figure S9.  $^1\text{H}$ - $^{13}\text{C}$  HSQC NMR spectrum of **3** in DMSO.



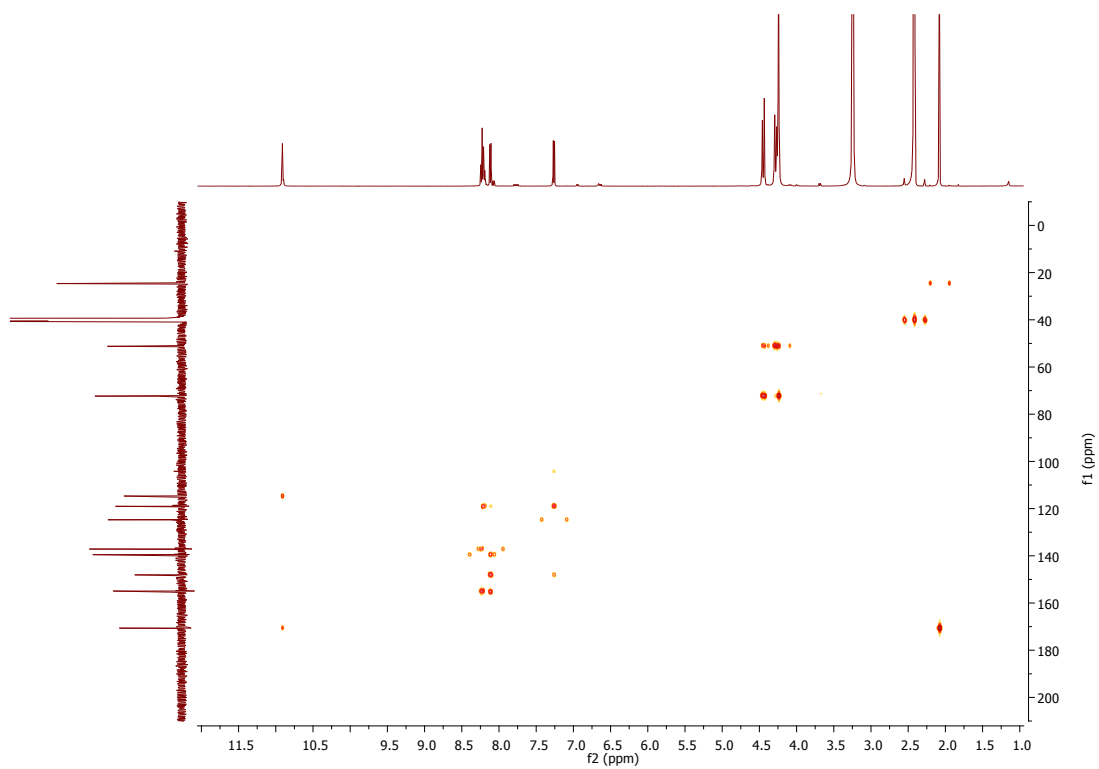


Figure S10.  $^1\text{H}$ - $^{13}\text{C}$  HMBC NMR spectrum of **3** in DMSO.

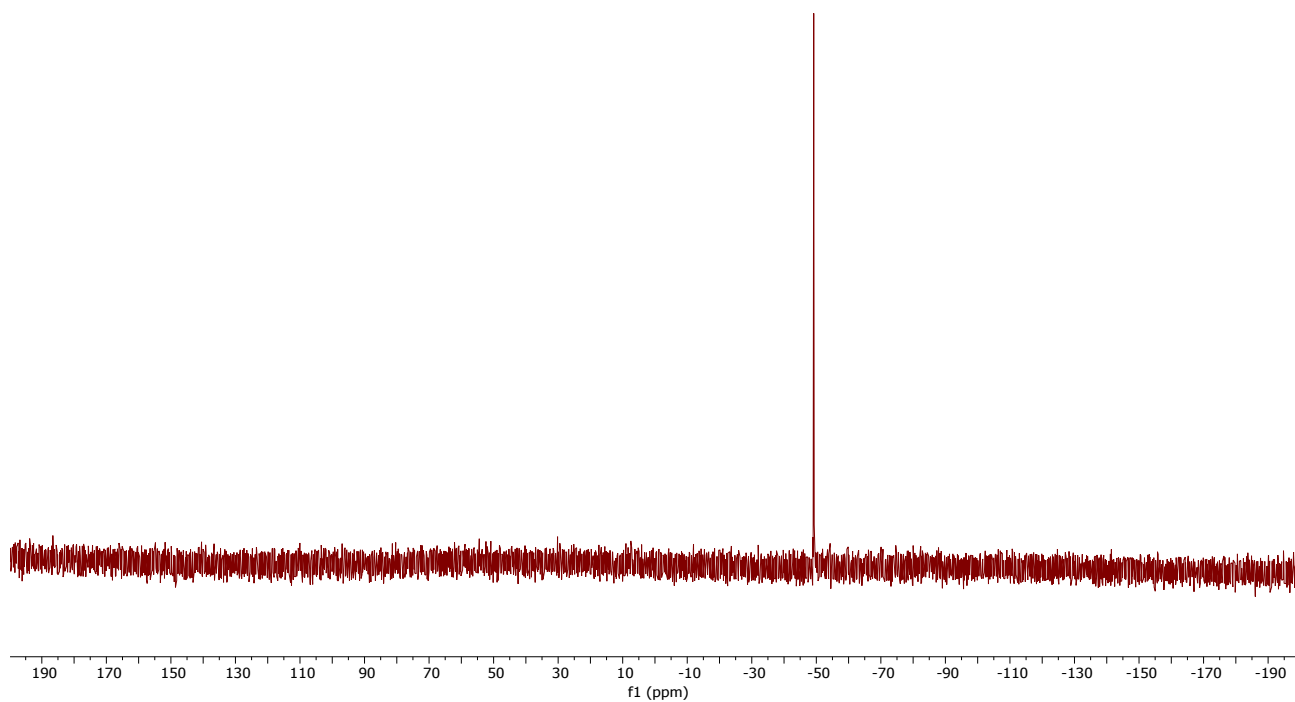
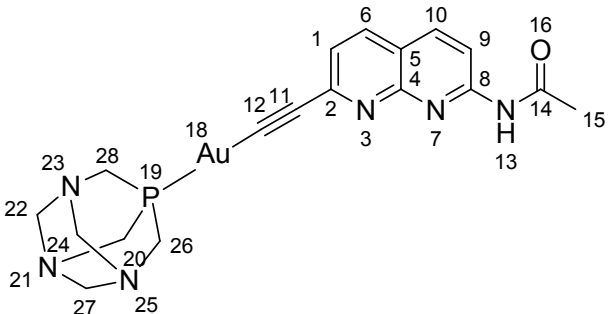
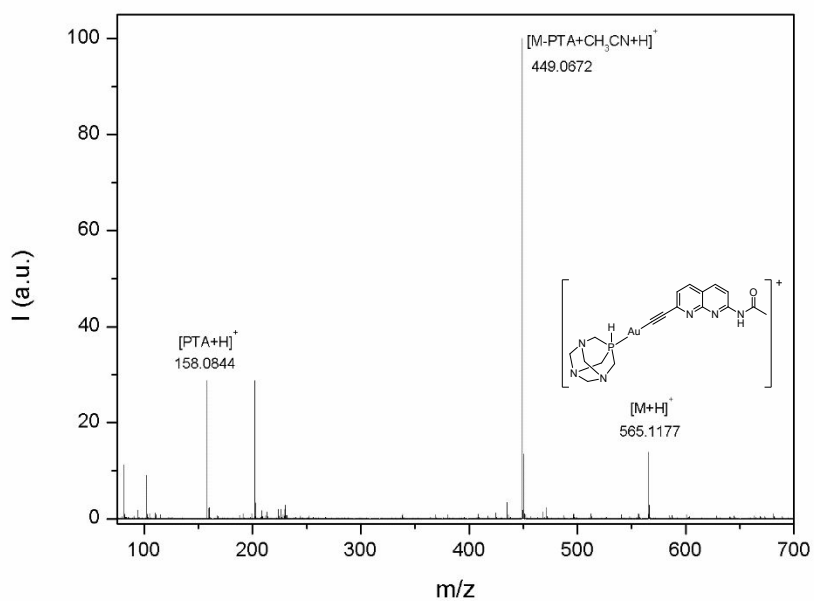
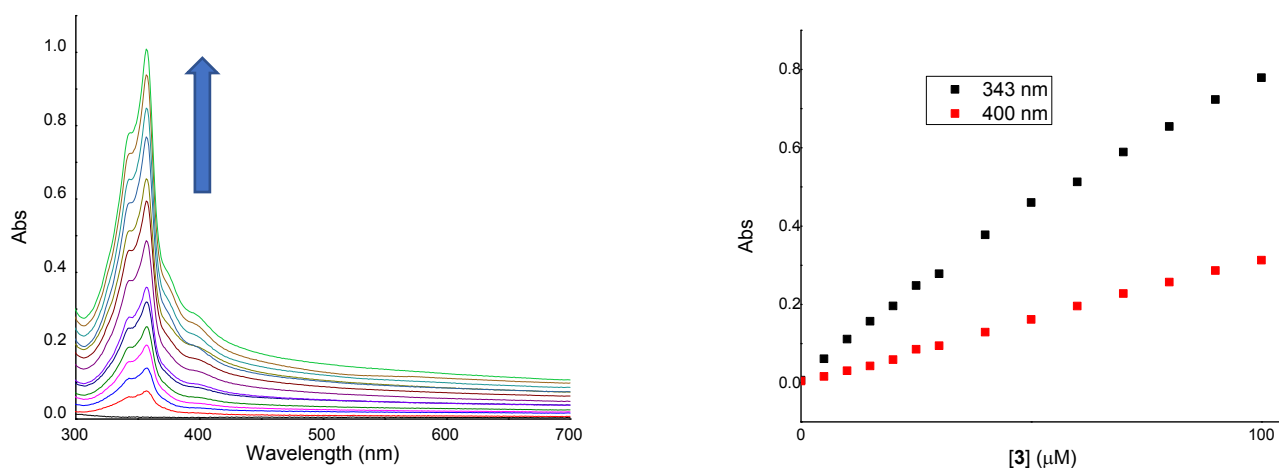


Figure S11.  $^{31}\text{P}$  NMR spectrum of **3** in DMSO.

Table S2. NMR peak assignment for **3**.


Position	<sup>1</sup> H	<sup>13</sup> C
1	7.26	124.72
2	-	148.07
3	-	-
4	-	155.24
5	-	119.02
6	8.12	137.13
7	-	-
8	-	154.93
9	8.24-8.19	114.67
10	8.24-8.19	139.51
11	-	-*
12	-	-*
13	10.91	-
14	-	170.64
15	2.08	24.64
16	-	-
17	-	-
18	-	-
19	-	-
20	4.45/4.28**	72.27
21	-	-
22	4.24	51.23/51.07**
23	-	-
24	4.24	51.23/51.07**
25	-	-
26	4.45/4.28**	72.27
27	4.24	51.23/51.07**
28	4.45/4.28**	72.27

\*These quaternary carbons were not observed, possibly due to (1) low relaxation times or (2) low sample concentration; \*\*Unequivocal assignment of these signals was not possible on the acquired spectra.

Figure S12. HR-MS spectrum of **3**.Figure S13. UV-Vis spectra at different concentrations of **3** in water (left); variations of absorbance at 343 nm and 400 nm at different concentrations of **3** (right).

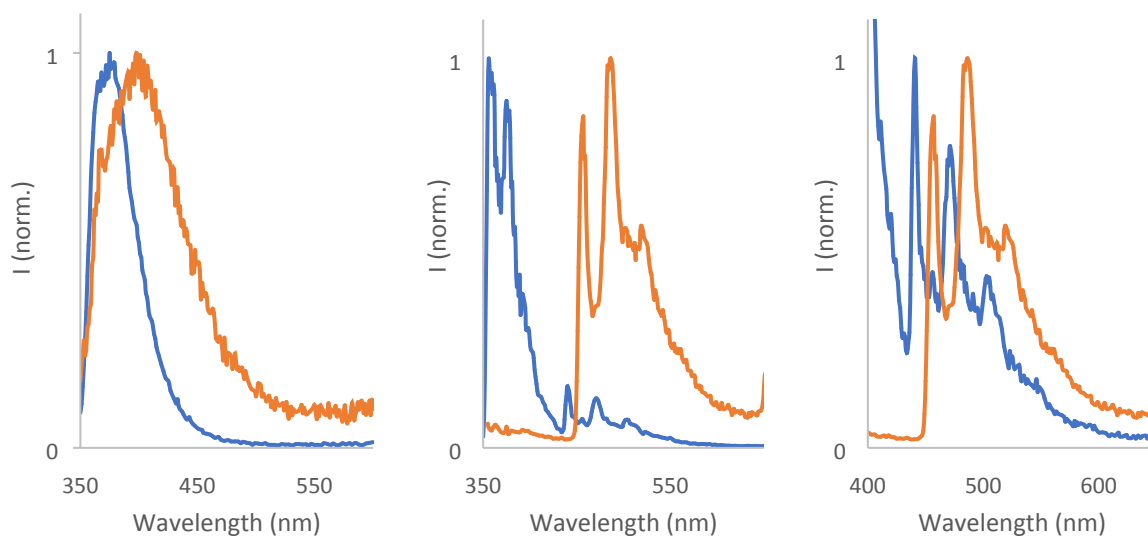


Figure S14. Left: Emission spectra of **2** (blue) and **3** (orange) in methanol at room temperature; Center: Normalized emission of **2** and **3** at 77K; Right: normalized spectra of **2** and **3** in the region between 400-650nm at 77K, for better comparison of the vibrational structure of the bands ( $\lambda_{\text{exc}} = 343$  nm for all cases).

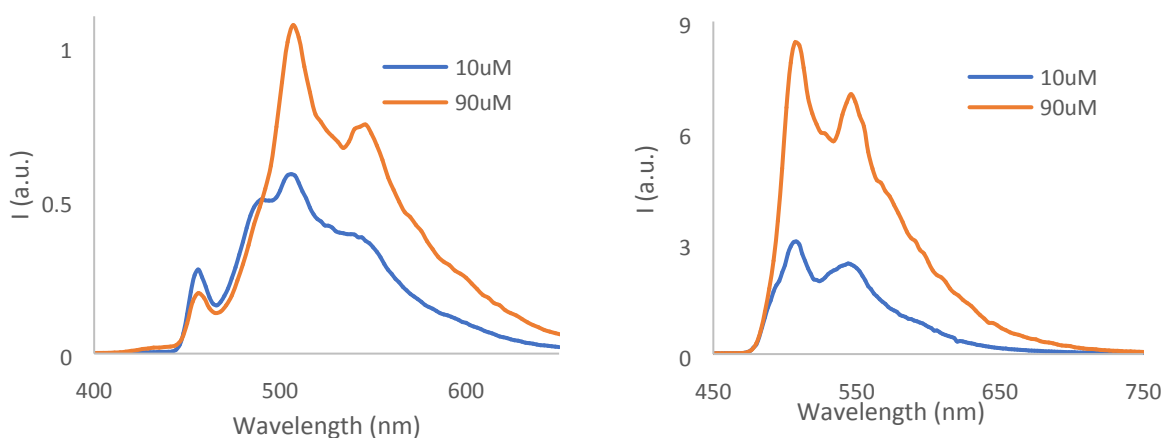


Figure S15. Emission spectra of 10 and 90  $\mu\text{M}$  solutions of **3** at 77K in 10 mM HEPES buffer (pH 7.2), exciting at 343 nm (left) and 400 nm (right).

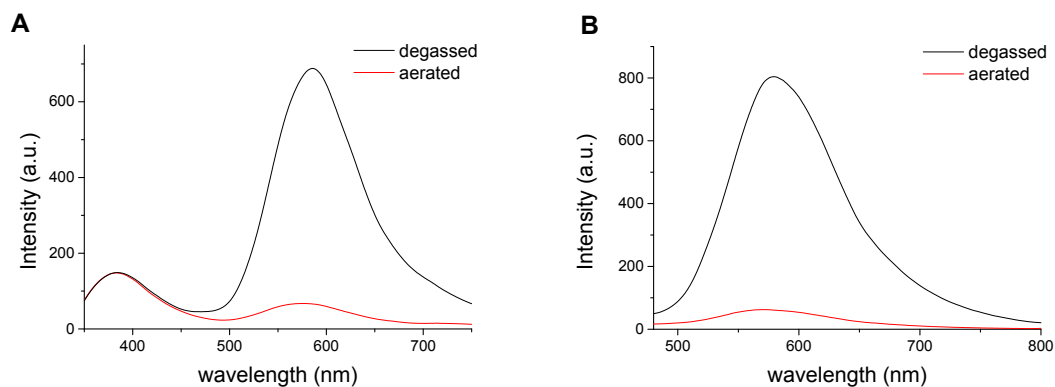


Figure S16. Steady-state emission spectra of a solid sample (powder) of **3** at room temperature in degassed (black line) and aerated (red line) conditions, exciting at (A) 320 nm and (B) 400 nm.

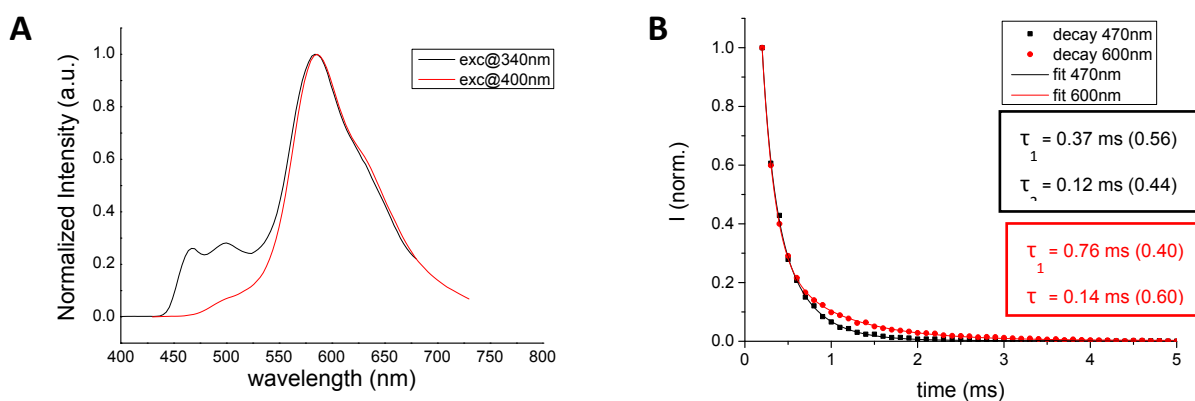


Figure S17. (A) Time-resolved emission spectra of **3** in solid state, exciting at 340 nm (black) and 400 nm (red). Delay = 0.2 ms; (B) decay profiles of the emission at 470 nm (black) and 600 nm (red). The contributions of each lifetime component are presented in brackets ( $\tau_{\text{average}} = 0.2$  ms). Excitation wavelength was 320 nm.

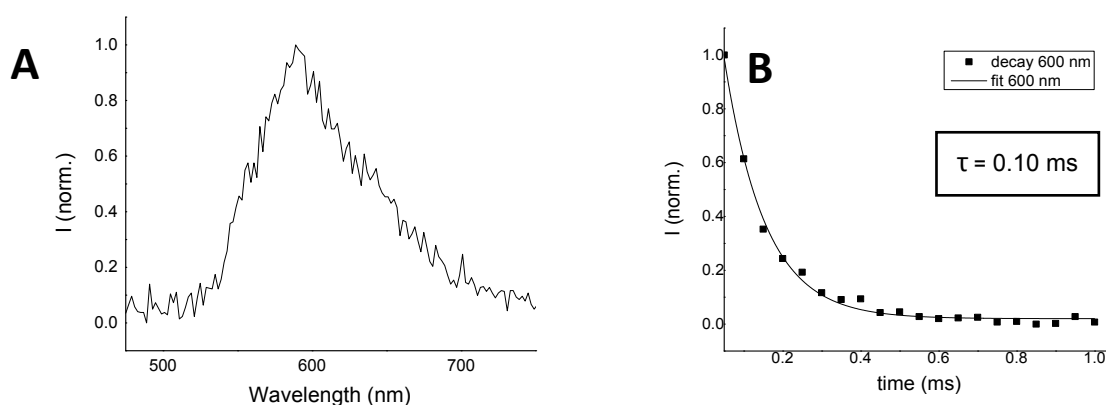


Figure S18. (A) Time-resolved emission spectra of **3** in 10mM HEPES buffer (pH7.2),  $\lambda_{\text{excitation}} = 400$  nm, delay = 0.2 ms. (B) Decay profile of the emission at 600 nm.

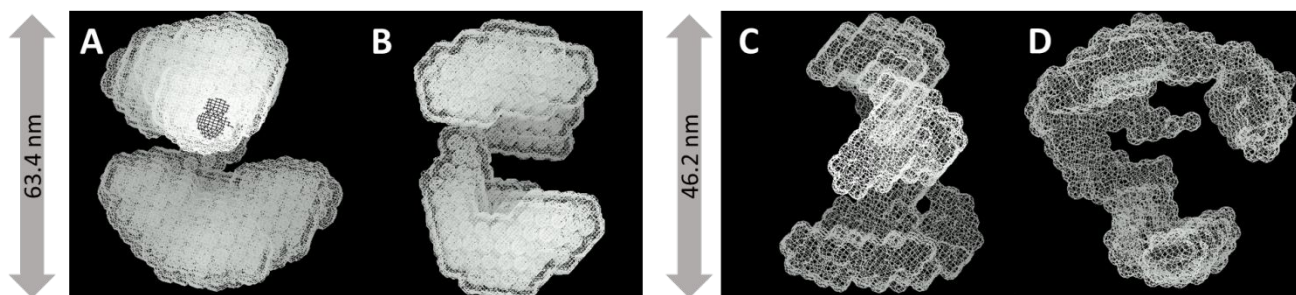


Figure S19. Low resolution structures obtained from SAXS measurements of **3** at  $1 \times 10^{-5}$  M in 100% DMSO (A and B) and 10% DMSO/90% H<sub>2</sub>O mixture (C and D). The pairs A/B and C/D represent the same structure at two different views, shifted by 90°.

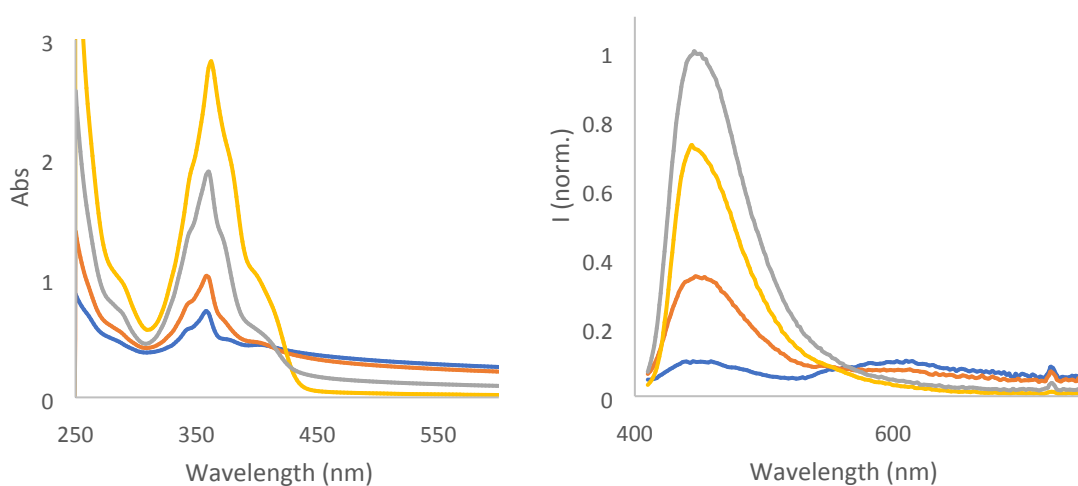


Figure 20. Absorption and emission ( $\lambda_{\text{exc}} = 410$  nm) of **3** ( $60 \mu\text{M}$ ) in different H<sub>2</sub>O:DMSO mixtures: 100% water (blue), 90% water:10% DMSO (red), 75% water:25% DMSO (grey), and 50% water:50% DMSO (orange).

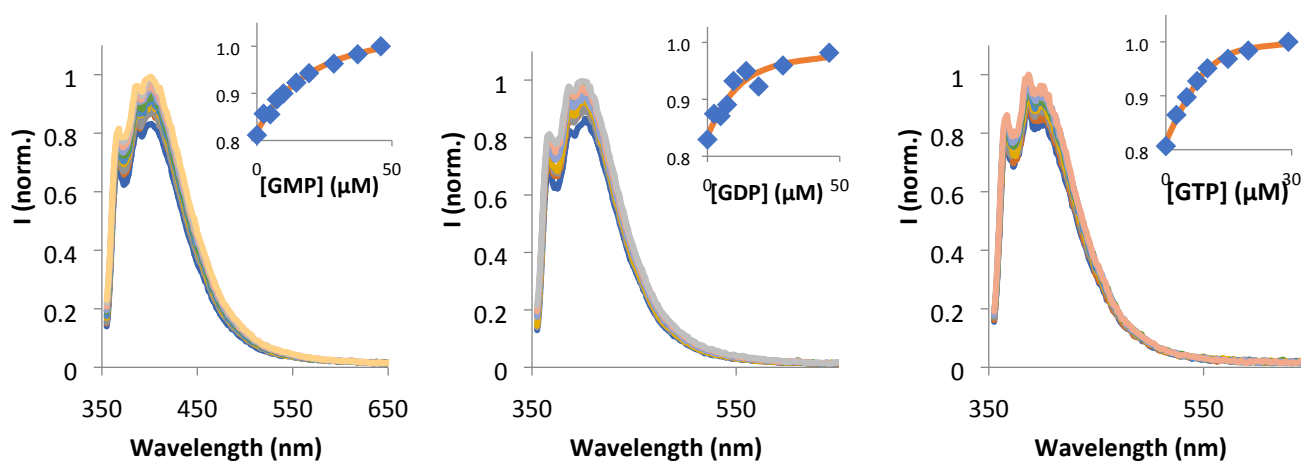


Figure S21. Emission spectra of **3** ( $10 \mu\text{M}$ , in 10mM HEPES buffer at pH 7.2) in the presence of different amounts of Guanosine nucleotides,  $\lambda_{\text{exc}} = 343$  nm. Insets show the trend of the normalized intensity versus concentration of respective Guanosine derivative.

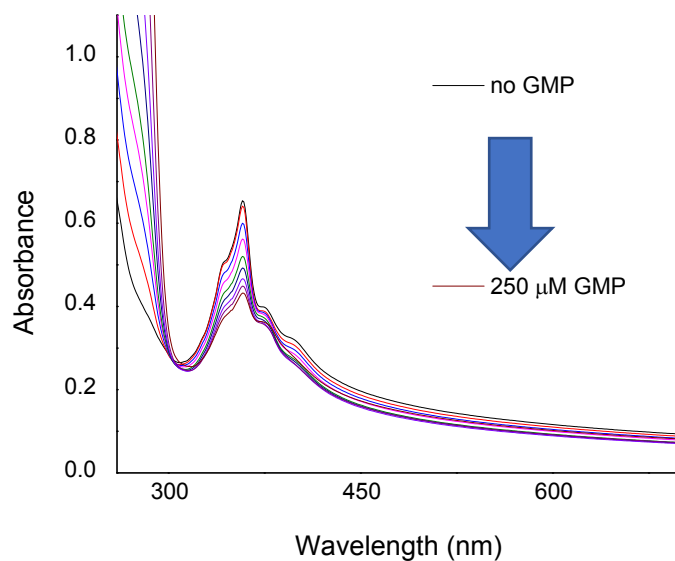


Figure S22. Variation of absorption of **3** ( $60\ \mu\text{M}$  in  $10\ \text{mM}$  HEPES buffer at  $\text{pH}\ 7.2$ ) in the presence of Guanosine 5'-monophosphate (GMP).

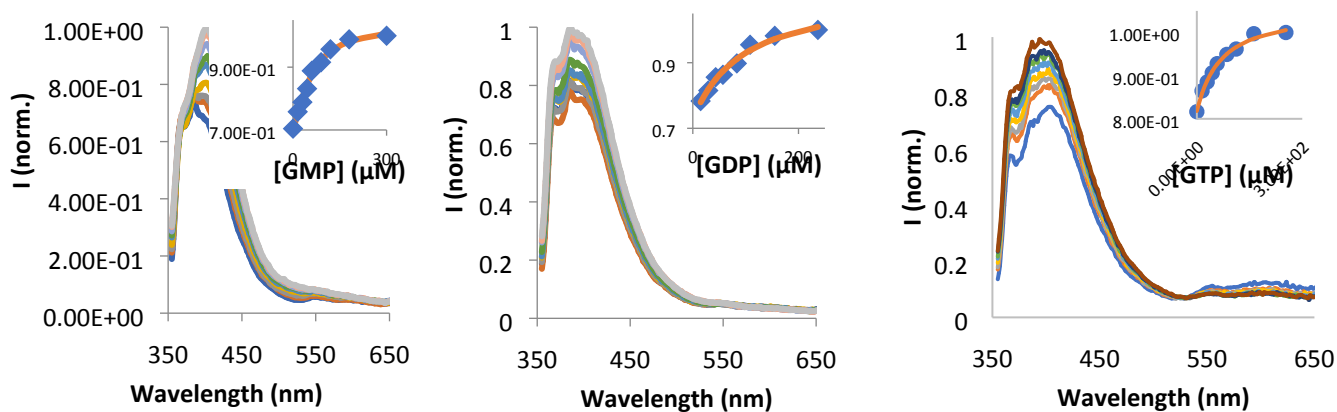


Figure S23. Emission spectra of **3** ( $60\ \mu\text{M}$ , in  $10\ \text{mM}$  HEPES buffer at  $\text{pH}\ 7.2$ ) in the presence of different amounts of Guanosine nucleotides,  $\lambda_{\text{exc}} = 343\ \text{nm}$ . Insets show the trend of the normalized intensity versus concentration of respective Guanosine derivative.

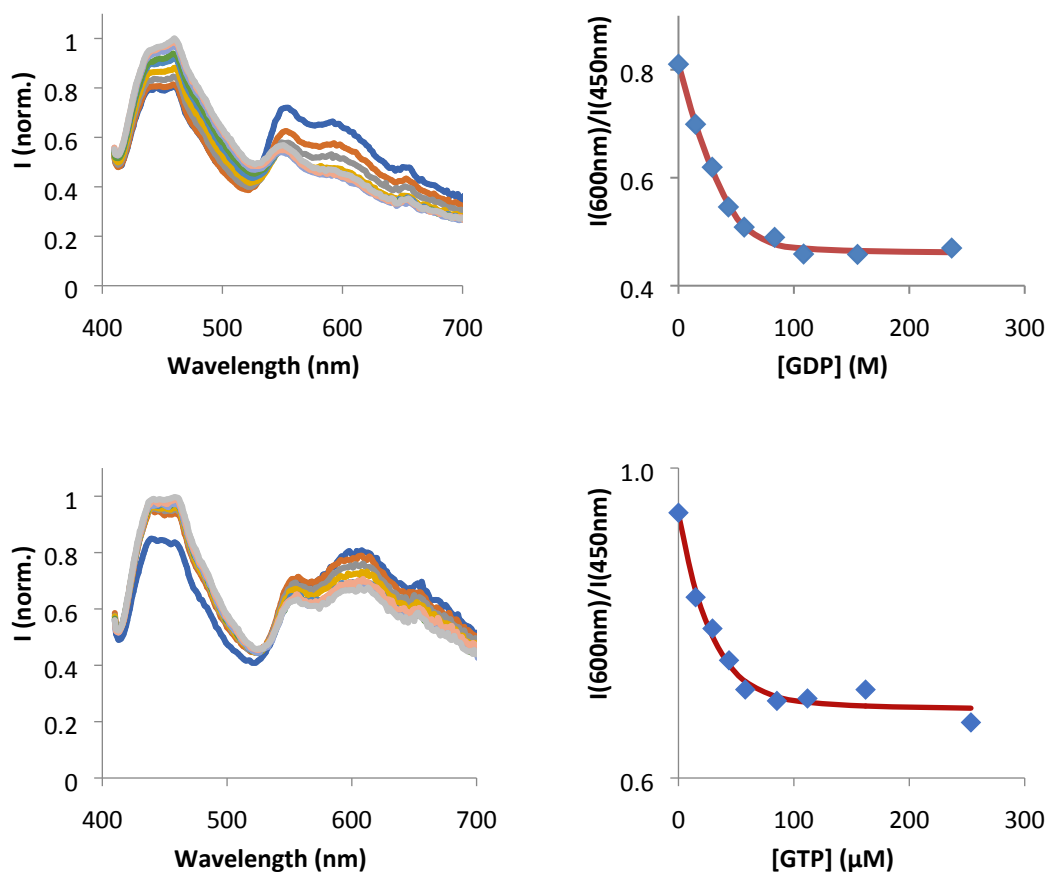


Figure S24. Emission spectra of **3** ( $60\mu\text{M}$ ) in the presence of different amounts of GDP (left, top) and GTP (left, bottom). Respective insets of the ratio between the monomer and aggregates emission are shown on the right

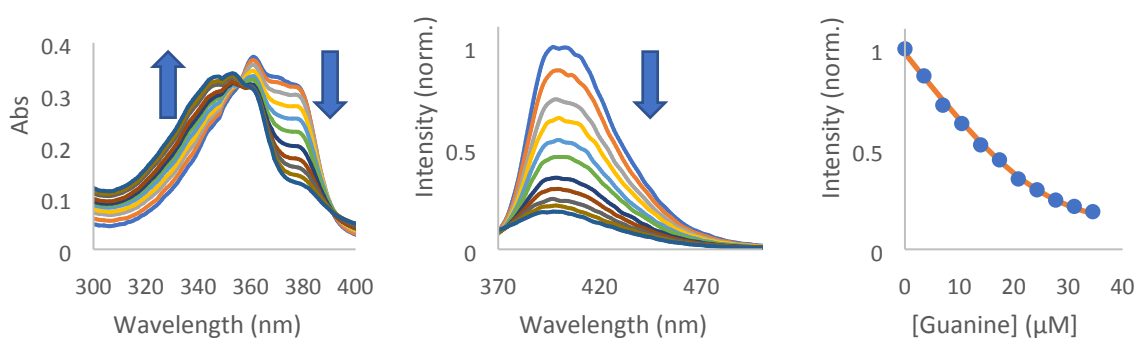


Figure S25. Absorption and emission ( $\lambda_{\text{exc}} = 372\text{ nm}$ ) spectra of **2** in dichloromethane ( $1 \times 10^{-5}\text{ M}$ ), in the presence of increasing amounts of Guanine. The association constant was determined by fitting the experimental data to a 1:1 Henderson-Hasselbalch model using the Solver Add-In from Microsoft Excel, yielding a value of  $4.2 \times 10^5\text{ M}^{-1}$ .



Table S3. Association constants for naphthyridine sensor systems towards Guanine derivatives reported in the literature.

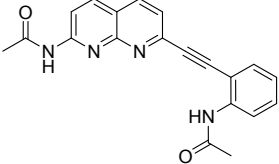
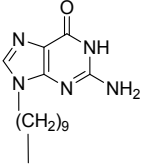
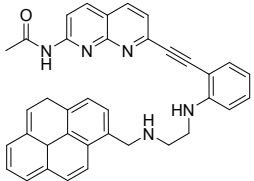
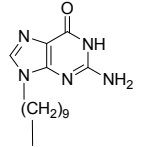
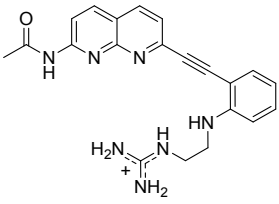
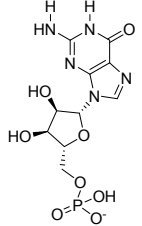
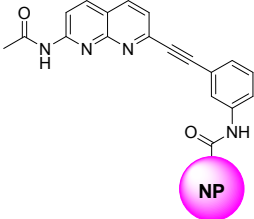
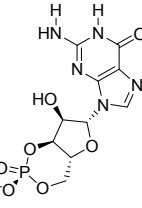
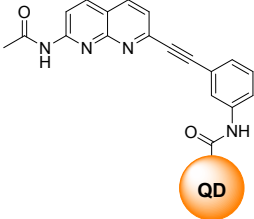
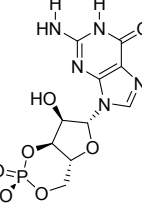
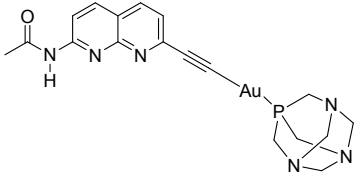
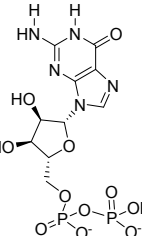
Sensor molecule	Analyte	$K_{\text{ass}} \text{ (M}^{-1}\text{)}$	Solvent	Reference
		$9.1 \times 10^4$	$\text{CH}_2\text{Cl}_2$	13
		$1.4 \times 10^6$	$\text{CH}_2\text{Cl}_2$	14
		$1.6 \times 10^4$	water	14
		$3.6 \times 10^4$	0.1M HEPES (pH7.4)	15
		$3.1 \times 10^5$	0.1M HEPES (pH7.4)	16
		$4.4 \times 10^5$	0.01M HEPES (pH7.4)	This work

Table S4. Crystal data and structure refinement for complex 3.

Empirical formula	C <sub>12</sub> H <sub>9</sub> N <sub>3</sub> O	
Formula weight	211.22	
Temperature	110(2) K	
Wavelength	0.71073 Å	
Crystal system	Monoclinic	
Space group	C 2/c	
Unit cell dimensions	a = 24.8320(8) Å	α = 90°.
	b = 7.2057(3) Å	β = 108.7530(10)°.
	c = 12.0342(4) Å	γ = 90°.
Volume	2038.99(13) Å <sup>3</sup>	
Z	8	
Density (calculated)	1.376 Mg/m <sup>3</sup>	
Absorption coefficient	0.092 mm <sup>-1</sup>	
F(000)	880	
Crystal size	0.200 x 0.100 x 0.100 mm <sup>3</sup>	
Theta range for data collection	3.466 to 25.700°.	
Index ranges	-28 ≤ h ≤ 30, -8 ≤ k ≤ 8, -14 ≤ l ≤ 14	
Reflections collected	16950	
Independent reflections	1931 [R(int) = 0.0313]	
Completeness to theta = 25.242°	99.5 %	
Refinement method	Full-matrix least-squares on F <sup>2</sup>	
Data / restraints / parameters	1931 / 0 / 150	
Goodness-of-fit on F <sup>2</sup>	1.081	
Final R indices [I > 2σ(I)]	R1 = 0.0351, wR2 = 0.0959	
R indices (all data)	R1 = 0.0410, wR2 = 0.0986	
Largest diff. peak and hole	0.257 and -0.217 e.Å <sup>-3</sup>	

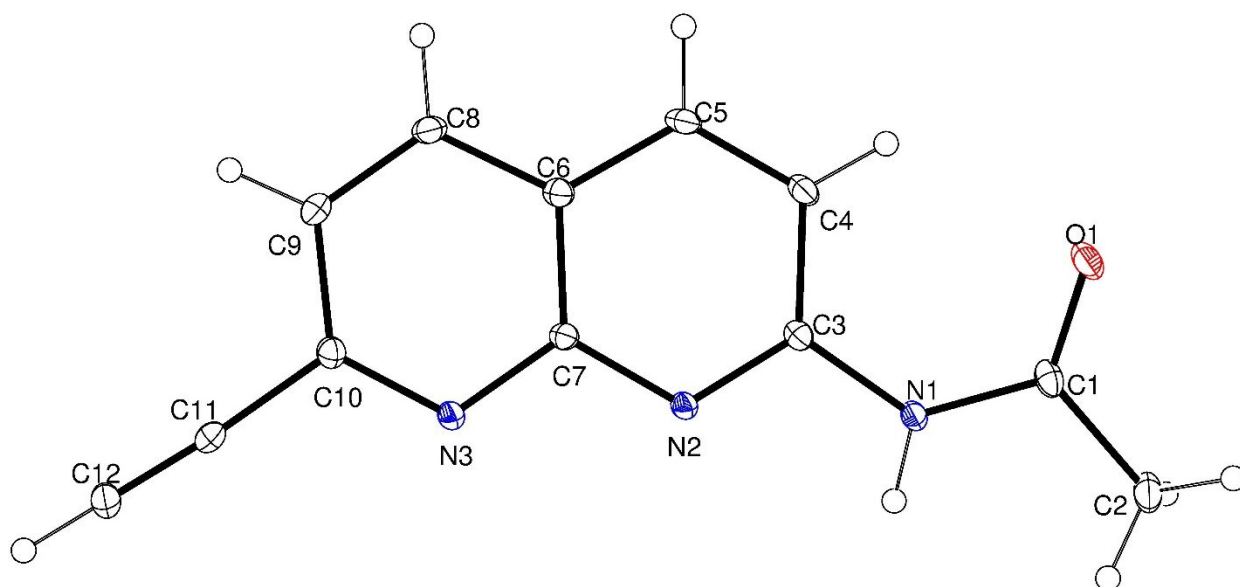


Fig. S25. ORTEP-3 diagram of complex 3, using 30% probability level ellipsoids.

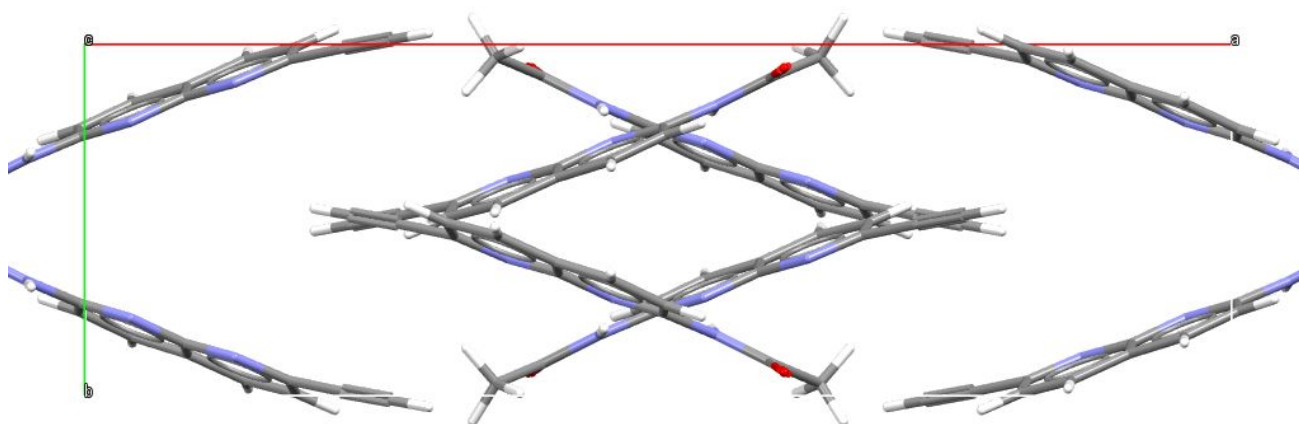


Fig. S26. MERCURY packing diagram viewed down the *c* axis.

Table S5. Atomic coordinates ( $\times 10^4$ ) and equivalent isotropic displacement parameters ( $\text{\AA}^2 \times 10^3$ ) for complex 3.  $U(\text{eq})$  is defined as one third of the trace of the orthogonalized  $U^{\text{ij}}$  tensor.

	x	y	z	$U(\text{eq})$
N(2)	9602(1)	2211(2)	1051(1)	14(1)
O(1)	11100(1)	4324(1)	659(1)	23(1)
C(8)	8604(1)	445(2)	-1725(1)	19(1)
N(3)	8693(1)	1098(2)	632(1)	15(1)
C(11)	7743(1)	114(2)	269(1)	18(1)
C(7)	9133(1)	1495(2)	234(1)	13(1)
N(1)	10510(1)	3271(2)	1640(1)	16(1)
C(6)	9108(1)	1195(2)	-943(1)	15(1)
C(4)	10058(1)	2408(2)	-445(1)	17(1)
C(5)	9591(1)	1684(2)	-1254(1)	18(1)
C(3)	10047(1)	2634(2)	725(1)	14(1)
C(10)	8221(1)	440(2)	-141(1)	16(1)
C(1)	11001(1)	4080(2)	1580(1)	18(1)
C(9)	8161(1)	77(2)	-1330(1)	19(1)
C(2)	11411(1)	4644(2)	2743(1)	23(1)
C(12)	7328(1)	-130(2)	534(1)	23(1)

Table S6. Bond lengths [ $\text{\AA}$ ] and angles [ $^\circ$ ] for complex 3.

N(2)-C(3)	1.3205(15)	N(3)-C(7)-C(6)	122.74(11)
N(2)-C(7)	1.3620(16)	N(2)-C(7)-C(6)	122.19(11)
O(1)-C(1)	1.2235(16)	C(1)-N(1)-C(3)	128.36(11)
C(8)-C(9)	1.3596(18)	C(1)-N(1)-H(1)	118.7(9)
C(8)-C(6)	1.4089(18)	C(3)-N(1)-H(1)	112.9(9)
C(8)-H(8)	0.9300	C(8)-C(6)-C(5)	124.49(11)
N(3)-C(10)	1.3286(16)	C(8)-C(6)-C(7)	118.10(11)
N(3)-C(7)	1.3566(15)	C(5)-C(6)-C(7)	117.41(11)
C(11)-C(12)	1.1855(18)	C(5)-C(4)-C(3)	118.01(11)
C(11)-C(10)	1.4428(17)	C(5)-C(4)-H(4)	121.0
C(7)-C(6)	1.4139(17)	C(3)-C(4)-H(4)	121.0
N(1)-C(1)	1.3735(16)	C(4)-C(5)-C(6)	120.57(11)
N(1)-C(3)	1.3901(16)	C(4)-C(5)-H(5)	119.7
N(1)-H(1)	0.891(16)	C(6)-C(5)-H(5)	119.7
C(6)-C(5)	1.4117(17)	N(2)-C(3)-N(1)	113.52(10)
C(4)-C(5)	1.3557(18)	N(2)-C(3)-C(4)	123.35(11)
C(4)-C(3)	1.4270(17)	N(1)-C(3)-C(4)	123.10(11)
C(4)-H(4)	0.9300	N(3)-C(10)-C(9)	123.83(11)
C(5)-H(5)	0.9300	N(3)-C(10)-C(11)	117.17(11)
C(10)-C(9)	1.4140(18)	C(9)-C(10)-C(11)	118.99(11)
C(1)-C(2)	1.4982(18)	O(1)-C(1)-N(1)	123.34(12)
C(9)-H(9)	0.9300	O(1)-C(1)-C(2)	122.18(11)
C(2)-H(2A)	0.9600	N(1)-C(1)-C(2)	114.49(11)
C(2)-H(2B)	0.9600	C(8)-C(9)-C(10)	118.94(12)
C(2)-H(2C)	0.9600	C(8)-C(9)-H(9)	120.5
C(12)-H(12)	0.9300	C(10)-C(9)-H(9)	120.5
C(3)-N(2)-C(7)	118.44(10)	C(1)-C(2)-H(2A)	109.5
C(9)-C(8)-C(6)	119.12(11)	C(1)-C(2)-H(2B)	109.5
C(9)-C(8)-H(8)	120.4	H(2A)-C(2)-H(2B)	109.5
C(6)-C(8)-H(8)	120.4	C(1)-C(2)-H(2C)	109.5
C(10)-N(3)-C(7)	117.23(10)	H(2A)-C(2)-H(2C)	109.5
C(12)-C(11)-C(10)	175.71(13)	H(2B)-C(2)-H(2C)	109.5
N(3)-C(7)-N(2)	115.06(10)	C(11)-C(12)-H(12)	180.0

Table S7. Torsion angles [°] for complex 3.

C(10)-N(3)-C(7)-N(2)	178.38(11)
C(10)-N(3)-C(7)-C(6)	-1.48(18)
C(3)-N(2)-C(7)-N(3)	-179.87(10)
C(3)-N(2)-C(7)-C(6)	-0.01(18)
C(9)-C(8)-C(6)-C(5)	-178.17(12)
C(9)-C(8)-C(6)-C(7)	1.34(19)
N(3)-C(7)-C(6)-C(8)	-0.26(19)
N(2)-C(7)-C(6)-C(8)	179.89(11)
N(3)-C(7)-C(6)-C(5)	179.28(11)
N(2)-C(7)-C(6)-C(5)	-0.57(18)
C(3)-C(4)-C(5)-C(6)	0.78(19)
C(8)-C(6)-C(5)-C(4)	179.65(12)
C(7)-C(6)-C(5)-C(4)	0.14(19)
C(7)-N(2)-C(3)-N(1)	-177.17(10)
C(7)-N(2)-C(3)-C(4)	1.03(18)
C(1)-N(1)-C(3)-N(2)	-169.36(12)
C(1)-N(1)-C(3)-C(4)	12.4(2)
C(5)-C(4)-C(3)-N(2)	-1.43(19)
C(5)-C(4)-C(3)-N(1)	176.59(12)
C(7)-N(3)-C(10)-C(9)	2.23(19)
C(7)-N(3)-C(10)-C(11)	-176.73(11)
C(3)-N(1)-C(1)-O(1)	-1.4(2)
C(3)-N(1)-C(1)-C(2)	178.74(12)
C(6)-C(8)-C(9)-C(10)	-0.68(19)
N(3)-C(10)-C(9)-C(8)	-1.2(2)
C(11)-C(10)-C(9)-C(8)	177.76(12)

Table S8. Hydrogen bonds for complex 3 [Å and °].

D-H	d(D-H)	d(H..A)	<DHA	d(D..A)	A
C4-H4	0.930	2.276	119.97	2.856	O1
N1-H1	0.891	2.097	170.85	2.980	N2 [ -x+2, y, -z+1/

Table S9: XYZ coordinates and energies of adducts 6A and 6B models (kcal/mol)

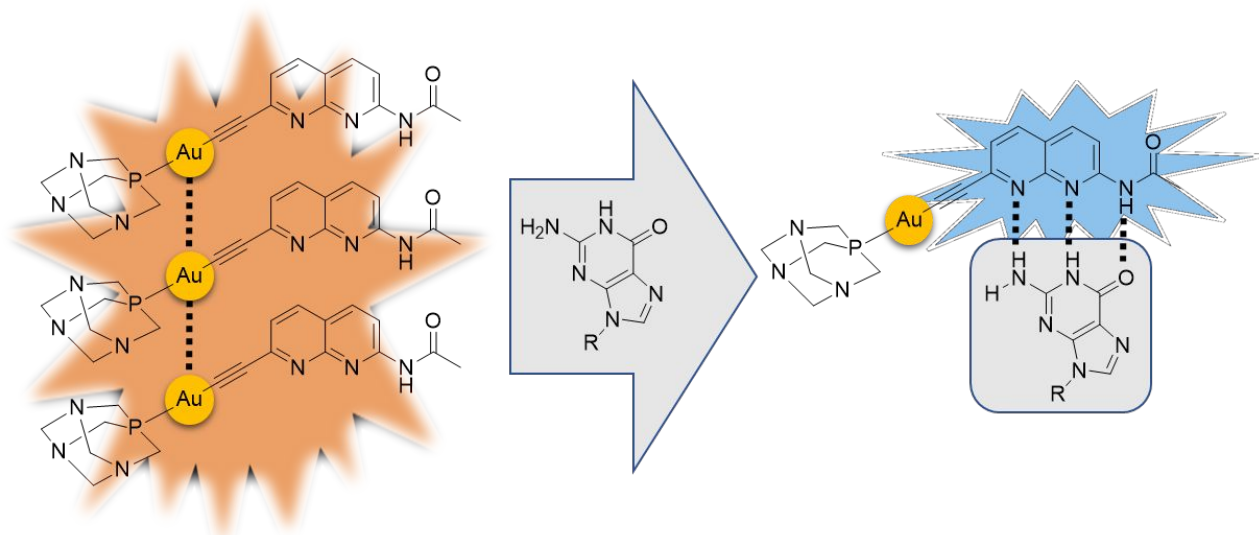
6A (-6270.17)			
1.C	-7.861468	1.232261	0.131439
2.C	-11.559018	3.174104	-0.141281
3.C	-12.677393	2.367529	-0.172148
4.C	-12.500427	0.957529	-0.109039
5.N	-11.297241	0.370186	-0.021591
6.C	-7.862769	2.668720	0.077668
7.C	-9.062212	3.323399	-0.010897
8.C	-10.277456	2.589090	-0.048994
9.C	-10.183892	1.155638	0.009620
10.N	-8.990816	0.508779	0.098260
11.H	-11.651699	4.257752	-0.187283
12.H	-13.679991	2.777286	-0.242585
13.C	-13.646252	0.100321	-0.138896
14.H	-9.093995	4.410721	-0.053644
15.H	-6.913100	3.186319	0.107738
16.C	-14.626728	-0.607493	-0.165395
17.H	-15.491653	-1.232112	-0.187660
18.N	-6.692753	0.499088	0.220823
19.C	-5.371781	0.966793	0.282362
20.C	-4.347672	-0.146195	0.434262
21.O	-5.060949	2.154395	0.241251
22.H	-3.364743	0.249802	0.171814
23.H	-4.596089	-1.024186	-0.168767
24.H	-4.331171	-0.474814	1.482012
25.H	-6.810179	-0.539070	0.234685
26.N	-9.015048	-2.518943	0.124360
27.C	-10.178220	-3.264944	0.065738
28.N	-10.187063	-4.596705	0.019975
29.C	-8.947757	-5.132415	0.043877
30.C	-7.703754	-4.476128	0.109132
31.C	-7.698592	-3.046205	0.154017
32.N	-8.634525	-6.476388	0.009105
33.C	-7.241038	-6.571676	0.055854
34.N	-6.657130	-5.395735	0.115639
35.O	-6.723473	-2.271150	0.211657
36.N	-11.341985	-2.575150	0.067889
37.H	-9.073734	-1.484168	0.137318
38.H	-9.306026	-7.234043	-0.037848
39.H	-6.737946	-7.530882	0.041395
40.H	-12.196207	-3.105023	-0.030597
41.H	-11.358440	-1.546859	0.034660

6B (-6244.99)			
1.C	-7.958065	1.663219	0.212870
2.C	-11.719758	3.334714	-0.417584
3.C	-12.770198	2.448592	-0.482707
4.C	-12.506228	1.054630	-0.318989
5.N	-11.278261	0.560557	-0.122851
6.C	-8.031265	3.086880	0.118014
7.C	-9.258661	3.669853	-0.089006
8.C	-10.408101	2.846036	-0.202042
9.C	-10.225035	1.424064	-0.075013
10.N	-9.003695	0.862667	0.133423
11.H	-11.884941	4.405296	-0.526302
12.H	-13.790832	2.780173	-0.646573
13.C	-13.590207	0.122756	-0.358615
14.H	-9.358210	4.750011	-0.178006
15.H	-7.125365	3.684167	0.185788
16.C	-14.513247	-0.657299	-0.396017
17.H	-15.315809	-1.360158	-0.431915
18.N	-6.692508	1.073798	0.450427
19.C	-6.150806	-0.029902	-0.216963
20.C	-4.882783	-0.585857	0.417575
21.O	-6.649736	-0.510411	-1.224247
22.H	-5.128331	-1.569137	0.837203
23.H	-4.472966	0.044786	1.213523
24.H	-4.128534	-0.735426	-0.361064
25.H	-6.079094	1.566581	1.089588
26.N	-8.146014	-5.076912	0.010576
27.C	-7.861779	-3.781497	-0.369635
28.N	-8.719088	-2.793693	-0.246159
29.C	-9.904507	-3.171004	0.298164
30.C	-10.313376	-4.451603	0.718016
31.C	-9.391107	-5.551388	0.594133
32.N	-10.977836	-2.345057	0.530694
33.C	-11.977020	-3.142852	1.071812
34.N	-11.617258	-4.407580	1.202126
35.O	-9.493396	-6.738358	0.891388
36.N	-6.587279	-3.511957	-0.849455
37.H	-7.429844	-5.796502	-0.052216
38.H	-11.021770	-1.340195	0.302432
39.H	-12.940904	-2.731368	1.343497
40.H	-6.526546	-2.570867	-1.249053
41.H	-6.150734	-4.236014	-1.411244

## Table of Contents (TOC)

# Aggregation Induced Emission from a new Naphthyridine-Gold(I) Complex as a potential tool for sensing Guanosine Nucleotides in Aqueous Media

Artur J. Moro,<sup>a\*</sup> João Avó,<sup>b</sup> Marc Malfois,<sup>c</sup> Francesco Zaccaria,<sup>d</sup> Célia Fonseca Guerra,<sup>d</sup>  
Francisco J. Caparrós,<sup>e,f</sup> Laura Rodríguez,<sup>e,f</sup> and João Carlos Lima<sup>a</sup>



A new organometallic alkynyl-gold(I) complex, bearing a naphthyridine fluorophore is herein presented. The complex is shown to exhibit Aggregation Induced Emission, which is disrupted in the presence of Guanosine nucleotides, via complementary hydrogen bonding with the naphthyridine group in aqueous environment, attesting its potential as luminescent sensor for these nucleotides.



# Aggregation Induced Emission from a new Naphthyridine-ethynyl-Gold(I) Complex as a potential tool for sensing Guanosine Nucleotides in Aqueous Media

Artur J. Moro,<sup>a\*</sup> João Avó,<sup>b</sup> Marc Malfois,<sup>c</sup> Francesco Zaccaria,<sup>d,e</sup> Célia Fonseca Guerra,<sup>d,f</sup>  
Francisco J. Caparrós,<sup>g,h</sup> Laura Rodríguez,<sup>g,h</sup> and João Carlos Lima<sup>a</sup>

<sup>a</sup> *LAQV-REQUIMTE, Departamento de Química, CQFB, Universidade Nova de Lisboa, Monte de Caparica, Portugal. E-mail:ajm12769@fct.unl.pt*

<sup>b</sup> *Instituto Superior Técnico, Universidade de Lisboa,*

<sup>c</sup> *ALBA Synchrotron Light Laboratory (CELLS), Carrer de la Llum 2–26, 08290 Cerdanyola del Vallès, Barcelona, Spain*

<sup>d</sup> *Department of Theoretical Chemistry, Amsterdam Center for Multiscale Modeling, Vrije Universiteit Amsterdam, De Boelelaan 1083, 1081 HV Amsterdam, The Netherlands*

<sup>e</sup> *Present address: Department of Nanochemistry, Istituto Italiano di Tecnologia, Via Morego 30, 16163, Genova, Italy*

<sup>f</sup> *Leiden Institute of Chemistry, Gorlaeus Laboratories, Leiden University, Einsteinweg 55, 2333 CC Leiden, The Netherlands.*

<sup>g</sup> *Departament de Química Inorgànica i Orgànica. Secció de Química Inorgànica. Universitat de Barcelona, Martí i Franquès 1-11, 08028 Barcelona, Spain.*

<sup>h</sup> *Institut de Nanociència i Nanotecnologia (IN<sup>2</sup>UB). Universitat de Barcelona, 08028 Barcelona (Spain)*

## Abstract

A new organometallic alkynyl-gold(I) complex, capable of exhibiting Aggregation Induced Emission was designed and synthesized. The linear complex structure possesses a central Au(I) atom, bearing two axial ligands: (1) 1,3,5-Triaza-7-phosphaadamantane; and (2) 2-acetamido-7-ethynyl-1,8-naphthyridine. While the former accounts for its partial solubility in aqueous environment, the latter acts as a receptor unit for binding guanosine nucleotides and derivatives via multiple hydrogen bonding. At high concentrations, aggregation of the complex was observed by the formation of new absorption ( $\lambda_{\text{max}} \sim 400$  nm) and emission bands (550-700 nm). Formation of aggregates of *ca.* 60 nm diameter was confirmed with Small Angle X-Ray Scattering (SAXS). Disruption of the aggregates in the presence of guanosine derivatives resulted in a ratiometric signal with apparent association constants in the order of  $10^5$  M<sup>-1</sup> and high sensitivity (around 63% signal change) which are, to the best of our knowledge, in line with the highest recorded for nucleotide sensing based on hydrogen bonding that are capable of working in water. Computational studies indicate the presence of additional hydrogen bonding interactions that account for the strong binding of the Au(I) complex to phosphorylated Guanosine nucleotides.

**Keywords:** naphthyridine; gold(I) complexes; guanosine sensors; Aggregation Induced Emission.

## 1. Introduction

Over the past years, research on alkynyl-gold(I) complexes (AGCs) has experienced a significant growth, mainly due to their luminescent properties, which confers them with outstanding potential for several applications, including molecular electronics and materials science.<sup>1-3</sup>

AGCs are linear complexes, with a central Au(I) bound to two axial ligands, one of which is a terminal alkyne. The general strategy for obtaining luminescent AGCs relies on the fact that one of the ligands is, in fact, a fluorophore by itself whose triplet emission is strongly increased due to the strong heavy atom effect induced by Au(I) which favors Inter-System Crossing (ISC).<sup>1,4</sup>

A particular feature from AGCs that has attracted significant attention from several research groups is their ability to self-assemble in aqueous solution through the formation of intermolecular aurophilic bonds, i.e. between two Au(I) atoms<sup>5</sup>, which comparable to strong hydrogen bonds.<sup>6,7</sup> This self-assembly into larger supramolecular aggregates can promote additional interactions between alkynyl ligands from neighboring complexes, such as  $\pi$ - $\pi$  stacking, which can originate new luminescence bands, resulting in Aggregation Induced Emission (AIE).<sup>8,9</sup>

The structure of the alkynyl ligands strongly influences both the luminescence as well as the size and shape of the obtained supramolecules.<sup>10</sup> Furthermore, factors such as concentration, solvent polarity, temperature are known to have a significant impact on the kinetics and thermodynamics of aggregation process, which hinders the full control of this phenomenon.<sup>11</sup> Recently, our group has reported a series of AGCs bearing fluorophores capable of coordinating divalent metal ions.<sup>12</sup> AGCs were found to aggregate in aqueous medium, producing luminescent structures with red emission. However, upon addition of Zn(II), the aggregates were disrupted and recovered their non-aggregated optical properties. Moreover, further addition of a stronger chelating agent (cryptand) allowed for the aggregation to take place once more, thus proving the control of this phenomenon by external stimuli.

Taking this into account, we aim to use the same strategy, i.e. aggregation/de-aggregation as a tool for sensing Guanosine nucleotides based on complementary hydrogen bonding (Watson-Crick interactions). With this in mind, we designed a new AGC possessing a 2-

acetamido-1,8-naphthyridine ligand (fig. 1a), a fluorophore which is known to act as a template structure for fluorescent sensing of Guanosine derivatives, given the nearly perfect complementarity in hydrogen bonding with Guanine nucleobase (fig. 1b).

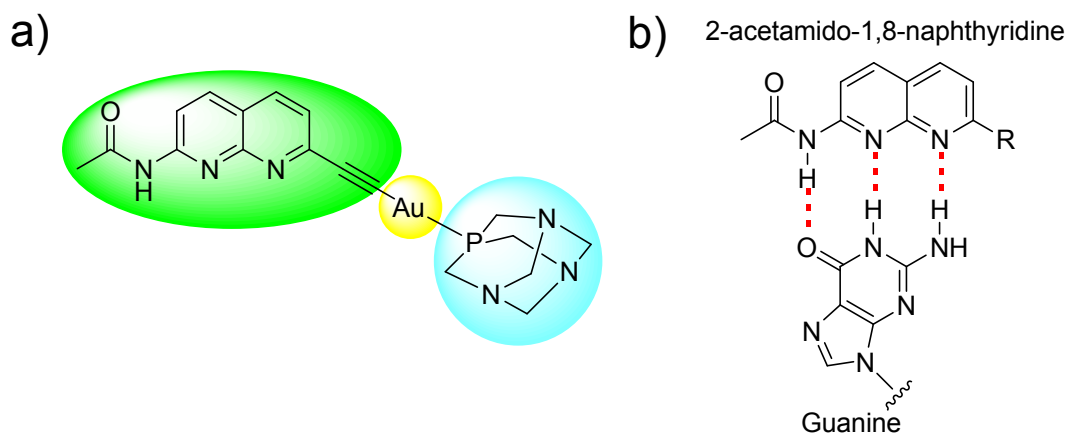


Figure 1. a) Structure of the designed AGC; b) Complementary hydrogen-bonding (red) between 2-acetamido-1,8-naphthyridine and guanine.

However, these sensor systems generally present poor water solubility and/or low sensitivity for detecting nucleotides in aqueous media, due to the competition of solvent molecules for the naphthyridine binding sites.<sup>13,14</sup> Only few systems capable of performing in water have been reported, and these require complex architectures (nanoparticles with embedded reference dyes/quantum dots) for obtaining a reproducible response.<sup>15,16</sup>

In this work, we designed an ethynyl-naphthyridine ligand and coupled it with a gold(I) complex, PTA–Au(I)–Cl (PTA = 1,3,5-Triaza-7-phosphaadamantane, highlighted in blue, figure 1a). The synthesis of this complex had three main goals: (1) to improve the solubility of the naphthyridine moiety in water, in order to perform binding with nucleotides in an aqueous environment, a desirable feature when considering biological applications; (2) to shift the luminescence properties to the visible/red region of the UV spectrum, as a result of its supramolecular self-assembling capabilities; (3) to assess the possibility of using the aggregation/de-aggregation capabilities to detect the presence of Guanosine derivatives, based on the complementary hydrogen bonding of the naphthyridine moiety.

## 2. Experimental

### 2.1. General

All solvents used were of spectroscopic grade. All reagents were purchased from Sigma-Aldrich and used as such without further purification. NMR spectra were recorded on a Bruker Advance III 400 spectrometer (400 MHz for  $^1\text{H}$ , 101 MHz for  $^{13}\text{C}$ , and 161.9 MHz for  $^{31}\text{P}$ ) at 298 K.

### 2.2. Synthesis

The synthesis of 2-acetamido-7-chloro-1,8-naphthyridine was performed according to reported literature procedures.<sup>17</sup>

#### 2.2.1. Synthesis of 2-acetamido-7-(ethynyl-[trimethylsilyl])-1,8-naphthyridine (**1**)

500 mg of 2-acetamido-7-chloro-1,8-naphthyridine (2.3 mmol), 226 mg of trimethylsilylacetylene (2.3 mmol), 62.8 mg of  $\text{PdCl}_2(\text{PPh}_3)_2$  (0.09 mmol) and 30.3 mg of  $\text{CuI}$  (0.16 mmol) were added to a 50 ml round-bottom flask equipped with a magnetic stirrer bar and a rubber seal. Under inert atmosphere, dry THF (12 ml) and dry triethylamine (3.39 ml, 24.3 mmol) were added to the flask. The reaction was left stirring overnight. The mixture was then filtered over a plug of celite and THF was removed in a rotary evaporator. The residue was purified on a Silica-Gel 60 flash chromatography (dichloromethane/acetone 9:1,  $R_f=0.31$ ), yielding 300 mg of pure **1** ( $\eta=47\%$ ).  $^1\text{H-NMR}$  (400 MHz,  $\text{CDCl}_3$ ):  $\delta$  9.79 (s, 1H), 8.57 (d,  $J = 8.9$  Hz, 1H), 8.18 (d,  $J = 8.9$  Hz, 1H), 8.09 (d,  $J = 8.2$  Hz, 1H), 7.52 (d,  $J = 8.2$  Hz, 1H), 2.36 (s, 3H), 0.31 (s, 9H).  $^{13}\text{C NMR}$  (101 MHz,  $\text{CDCl}_3$ )  $\delta$  170.36, 170.36, 154.81, 154.45, 146.26, 138.88, 136.63, 124.09, 119.89, 116.26, 103.87, 97.74, 25.11, -0.35.

#### 2.2.2. Synthesis of 2-acetamido-7-ethynyl-1,8-naphthyridine (**2**)

Compound **1** (280 mg, 0.99 mmol) was dissolved in a mixture of THF (10 ml) and water (1 ml). The solution was cooled to  $0^\circ\text{C}$  in an ice bath and tetrabutylammonium fluoride (2.2ml, from a 1M solution in THF) was added. The mixture was left to stir at room temperature until TLC revealed full consumption of the reagents (30 min.), at which point solvents were removed in a rotary evaporator. The residue was resuspended in  $\text{CH}_2\text{Cl}_2$  (10 ml), washed

with water (2x10 ml), brine (10 ml), dried with anhydrous  $\text{Na}_2\text{SO}_4$  and concentrated in a rotary evaporator. Silica-gel 60 flash chromatography ( $\text{CH}_2\text{Cl}_2$ :Acetone 4:1,  $R_f=0.3$ ) yielded 180 mg of **2** (86%) as a light brown powder. A small fraction was dissolved in  $\text{CHCl}_3$  which, by slow evaporation, resulted in the formation of crystals (see Supporting Information for crystallography data).  $^1\text{H}$  NMR (400 MHz, DMSO)  $\delta$  11.11 (s, 1H), 8.44 – 8.38 (m, 3H), 7.61 (d,  $J = 8.1$  Hz, 1H), 4.56 (s, 1H), 2.19 (s, 3H).  $^{13}\text{C}$  NMR (101 MHz, DMSO)  $\delta$  170.79, 155.47, 154.91, 145.42, 139.82, 138.24, 124.13, 120.13, 115.97, 83.98, 82.40, 24.68. Elemental analysis for  $\text{C}_{12}\text{H}_9\text{N}_3\text{O}$  (211.22): calcd C 68.24, H 4.29, N 19.89%; found: C 68.22, H 4.35, N 19.65%.

### 2.2.3. Synthesis of Au(I) complex (**3**)

Solid KOH (11.2 mg, 0.2 mmol) was added to a solution of **2** (22.5 mg, 0.1 mmol) in methanol (5 ml). After 5 min of stirring a dichloromethane solution (5 ml) of  $[\text{AuCl}(\text{PTA})]$  (39.0 mg, 0.1 mmol) was added and the solution was maintained at room temperature protected from light with aluminium foil. After 2 hours of stirring, the solution was concentrated to ca. 2 ml and hexane (5 ml) was added to precipitate a pale yellow solid which was filtered and obtained in 60% yield (34 mg, 0.06 mmol).  $^1\text{H}$  NMR (500 MHz, DMSO)  $\delta$  10.91 (s, 1H), 8.24 – 8.19 (m, 2H), 8.12 (d,  $J = 8.3$  Hz, 1H), 7.26 (d,  $J = 8.2$  Hz, 1H), 4.45 (d,  $J = 12.7$  Hz, 3H), 4.28 (d,  $J = 13.2$  Hz, 3H), 4.24 (s, 6H), 2.08 (s, 3H).  $^{13}\text{C}$  NMR (126 MHz, DMSO)  $\delta$  170.64, 155.24, 154.93, 148.07, 139.51, 137.13, 124.72, 119.02, 114.67, 72.27, 51.23, 51.07, 24.64.  $^{31}\text{P}\{^1\text{H}\}$  NMR (161.9 MHz, DMSO- $d_6$ , ppm): -49.2 (s). IR (KBr,  $\text{cm}^{-1}$ ): 2104 (C $\equiv$ C), 1641 (C=N). HR-ES-MS (+)  $m/z$ : 565.1177 ( $[\text{M} + \text{H}]^+$ , calc: 565.1180).

### 2.3. UV/Vis and fluorescence spectroscopies

Absorption spectra were obtained in a 1 cm quartz cuvette in acetonitrile on a Varian Cary 100 Bio UV- spectrophotometer. Emission spectra in solution were obtained in fluorescence quartz cuvette 1 cm, using a Horiba-Jobin-Yvon SPEX Fluorolog 3.22 spectrofluorimeter. Solid state emission spectra were acquired in the same apparatus, and the samples were obtained by dropcasting a acetonitrile solution onto a quartz plate. Luminescence measurements at 77K were performed in the same spectrofluorimeter, equipped with a cryogenic support with liquid nitrogen, in a glass tube. Association constants

were determined by fitting the experimental data to a 1:1 Henderson-Hasselbalch model using the Solver Add-In from Microsoft Excel.

#### 2.4. *Small-Angle X-Ray Scattering (SAXS)*

SAXS data have been performed on the NCD beamline at the synchrotron ALBA at 12.4 keV and the distance sample/detector was 2.2m to cover the range of momentum transfer  $0.09 < q < 5.6 \text{ nm}^{-1}$ . The data were collected on an ImXPad S1400 detector with a pixel size of  $130.0 \times 130.0 \mu\text{m}^2$ . The exposure time was 10s. The q-axis calibration was obtained by measuring silver behenate.<sup>18</sup> The program pyFAI<sup>19</sup> was used to integrate the 2D SAXS data into 1D data. The data were then subtracted by the background using *PRIMUS* software.<sup>20</sup> The maximum particle dimension  $D_{\text{max}}$  and the pair-distance distribution function  $P(r)$  were determined with *GNOM*.<sup>21</sup> The low-resolution structure of the aggregates was reconstructed ab initio from the initial portions of the scattering patterns using the program DAMMIN.<sup>22,23</sup>  $1 \cdot 10^{-4} \text{ M}$  and  $1 \cdot 10^{-5} \text{ M}$  solutions of complex **3** were prepared in two different water/DMSO mixtures: 90:10 and 0:100.

#### 2.5. *Computational Methods*

All calculations have been performed using the Amsterdam Density Functional (ADF) program and dispersion-corrected density functional theory (DFT-D3-BJ) at BLYP/TZ2P in gasphase. No symmetry constraint has been imposed. For interactions between ligand **2** and Guanine, only two matches have been reported since Guanine is characterized by a certain structural rigidity and therefore no other association could reasonably be probed.

$\Delta E_{\text{Bond}}$ , the energetic parameter hereby used to estimate the strength of the bonding between chemical structures is expressed as:

$$\Delta E_{\text{Bond}} = E_{\text{adduct}} - E_1 - E_2 \quad (\text{equation 1})$$

where  $E(\text{adduct})$  is the total bonding energy of the optimized complex and, in turn,  $E(\text{structure 1})$  and  $E(\text{structure 2})$  represents the energy of each of the chemical structures that compose the adduct, both individually optimized.





### 3. Results and Discussion

#### 3.1. Synthesis

The structure of Au(I) complex for sensing Guanosine nucleotides was designed to present (1) Aggregation Induced Emission (AIE) and (2) strong affinity to Guanosine derivatives via Watson-Crick base-pairing interactions. With respect to the first point, we selected a specific phosphine, namely 1,3,5-Triaza-7-phosphaadamantane (PTA), which coordinates with Au(I) atoms and is able to increase solubility of the final complex in water.<sup>24</sup> 2-acetamido-1,8-Naphthyridine chromophore was selected for its perfect triple-hydrogen bonding complementarity with Guanine nucleobase.<sup>12,13</sup> Figure 2 illustrates the full synthetic pathway for the desired Au(I) complex.

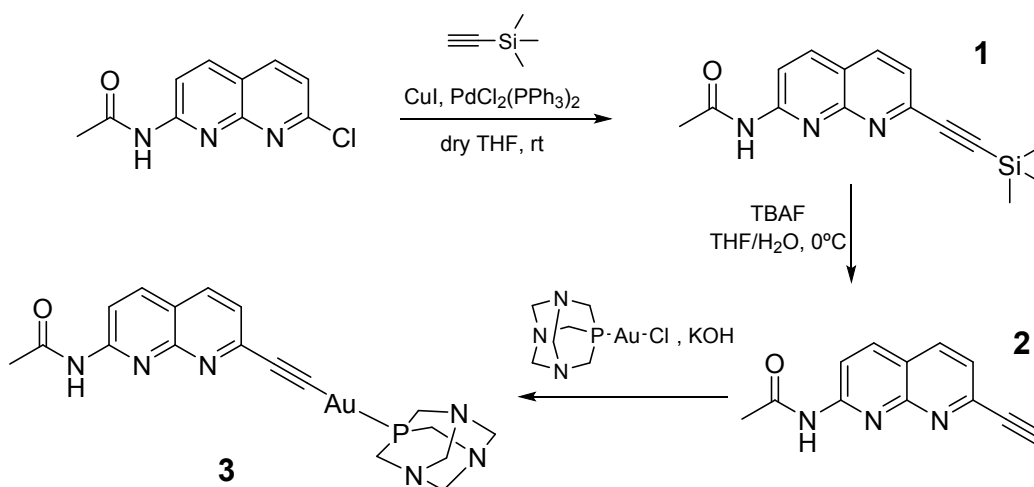


Figure 2. Synthetic pathway for obtaining PTA-Au(I)-(2-acetamido-7-ethynyl-1,8-naphthyridine) complex **3**.

The starting 2-acetamido-7-chloro-1,8-naphthyridine was synthesized according to previously established procedures.<sup>17</sup> Addition of an ethynyl moiety was performed via Sonogashira coupling with ethynyl-(trimethyl)silane (**1**), with subsequent removal of TMS with tetrabutylammonium fluoride, yielding crystals of compound **2** from chloroform (see Supporting Information for crystal data and NMR, figs. S1-S5 and tables S1, S4-S7). The obtained crystal structure shows a nearly perfect planarity of the naphthyridine moiety, ideal for the required complementarity with Guanine.

Converging synthesis with PTA-Au(I)-Cl in basic conditions<sup>25</sup> yielded the final complex **3** (NMR and HR-MS data is shown in figs. S6-S12 and table S2 of the Supplementary Information).

### 3.2. *Aggregation studies in water*

#### 3.2.1. *UV-Vis and fluorescence spectroscopy*

Given that detection of nucleotides is to be performed in aqueous media, the influence of concentration increase in the optical properties of **3** in water was assessed.

As can be seen in the UV-Vis spectra (fig. S13), upon increasing the concentration of **3**, an increase in the optical density at longer wavelengths (above 500 nm) is observed, which indicates a higher turbidity of the sample, a typical observation when precipitation or aggregation takes place.<sup>25</sup> Moreover, a band at around 400 nm becomes more prominent. The absorption from this band follows the same linear trend as the maximum absorption, and may be related to a metal-to-ligand- or ligand-to-metal-charge-transfer transition.

In the corresponding emission spectrum (fig. 3), if we excite the naphthyridine fluorophore at its strongest absorption band ( $\lambda_{\text{exc}} = 343$  nm, corresponding to the left shoulder of the band), we obtain a strong emission band with maximum intensity at 385 nm, corresponding to the fluorescence of naphthyridine, and low intensity bands at around 450 nm, 490 nm and 550 nm (fig. 3A). The overall intensity of the spectra reaches a plateau at concentrations above 50  $\mu\text{M}$ , probably due to the increase of inner-filter and self-quenching effects (fig. 3B).

When the sample is excited at  $\lambda_{\text{exc}} = 400$  nm, we obtain the previously observed band at 450 nm (fig. 3C), with a similar trend as the one shown in fig. 3B. Moreover, an increase in the intensity between 550 to 600 nm occurs along the studied concentration range, in two incremental steps (fig. 3D). Intersecting the linear trendlines from the two steps yields the Critical Aggregation Concentration (CAC), i.e., the concentration at which aggregation starts to occur, corresponding to 25.1  $\mu\text{M}$ . For this reason, this band was attributed to AIE from complex **3**.

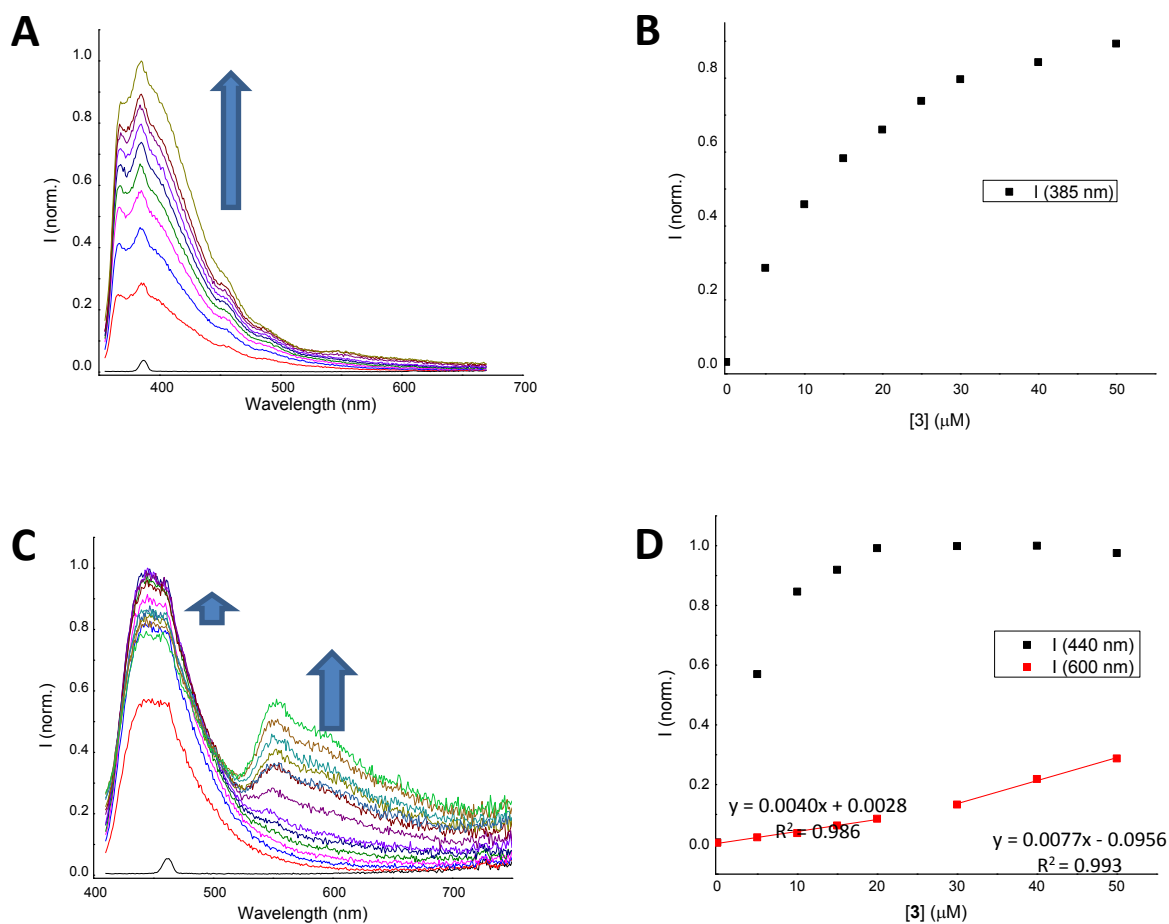


Figure 3. Emission spectra of **3** in water at different concentrations: (A) excitation at 343 nm or (C) 400 nm. Respective insets (B and D) show variations at the maximum peak of each spectrum.

In order to gain further insight on the origin of all the observed emission bands, emission spectra of **2** and **3** in methanol were recorded at room temperature and at 77K (fig. S14) (methanol was used due to poor water solubility of **2**).

At room temperature, the emission pattern of complex **3** was red-shifted by ca. 16-20 nm when compared to **2**. At 77K, ligand **2** exhibits the fluorescence band at 385 nm with vibrational structure, and an additional transition with vibrational resolution was observed with peaks at 441, 472 and 503 nm, tentatively assigned as triplet emission. In contrast, complex **3** displayed almost negligible fluorescence ( $\lambda_{\text{max}} \sim 395\text{nm}$ ), and a strong emission with vibrational structure in the range 440-600 nm. In fact, the vibrational structure of this emission is identical to the triplet emission of ligand **2**, although slightly red shifted (457,

486 and 519 nm). Therefore, this transition can be assigned as phosphorescence from the naphthyridine ligand, which is much more intense in complex **3** due to the heavy-atom effect induced by the Au(I) center, which promotes Inter-System Crossing (ISC) to the triplet state of the chromophore.

To better mimic the aggregation of **3** in aqueous solution observed in the emission spectra (see fig. 3C above), further experiments at 77K were performed in water. Figure S15 depicts the emission spectra obtained for an aqueous solution of **3** at 10  $\mu\text{M}$  and 90  $\mu\text{M}$  upon excitation at 343 nm and 400 nm. It is evidenced that the increase in concentration leads to a marked increase in the emission at 510 and 550 nm at both excitation wavelengths, while the emission below 500 nm does not change significantly. These results suggest that the complex spectra are composed by the phosphorescence of the “free” complex molecules, below 500 nm, and the phosphorescence of the aggregates, above 510 nm.

Steady-state emission spectra of **3** were also recorded in the solid state at room temperature. Excitation at 320 nm yielded emission bands at 383 and 600 nm, matching the monomer and aggregates bands recorded in solution, respectively (fig. S16A). Excitation at 400 nm yielded only the latter emission band (fig. S16B). This emission band was found to be highly sensitive to oxygen, increasing significantly upon degassing the sample. This suggests that the “aggregates” emission arises from triplet states and is either a delayed fluorescence (DF) or room-temperature phosphorescence (RTP).

Time-resolved spectra of **3** were also acquired, both in solid state and in aqueous solution (fig. S17 and S18). In the solid state, excitation at 320 nm reveals emission bands at 470 and 500 nm, and a strong emission at around 600 nm (identical to that of fig. S16). Decay analysis of emission maxima at 470 and 600 nm fit to a bi-exponential function, with a short lifetime similar for both wavelengths (0.12 and 0.14 ms for 470 and 600 nm, respectively, fig. S17B), and a longer lifetime component which is two times faster for 470 nm (0.37 ms) than for 600 nm (0.76 ms). These results suggest that the two emission bands arise from different states, and they can, thus, be attributed to the phosphorescence of “free” complex **3** and to the DF or RTP of the aggregates of complex **3**.

In solution, time-resolved spectra acquired at a concentration of 90  $\mu\text{M}$  revealed only the 600 nm emission, with a single exponential decay of 0.10 ms (fig. S18). Given the similarity in the location and lifetime of the bands with the solid state sample, this is a clear indication

that the red-shifted emission band observed in solution corresponds to the emission of higher aggregates.

### 3.2.2. Small-Angle X-Ray Scattering (SAXS)

The formation of aggregates was analyzed by SAXS. Measurements were performed for  $1 \times 10^{-5}$  and  $1 \times 10^{-4}$  M solutions of **3** in different H<sub>2</sub>O/DMSO proportions. Low-resolution structures were reconstructed *ab initio* from the scattering patterns using the DAMMIN program<sup>22,23</sup> (fig. 4 and S19).

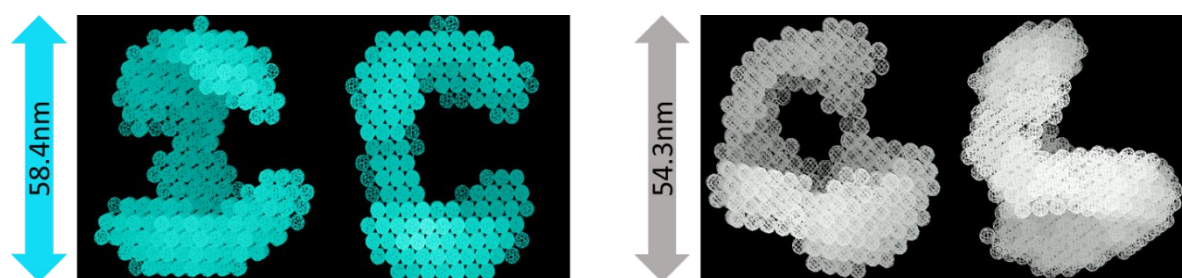


Figure 4. Low resolution structures obtained from SAXS measurements of **3** at  $1 \times 10^{-4}$  M in 100% DMSO (left, in blue) and 10% DMSO / 90% H<sub>2</sub>O mixture (right, white). Two views are shown, shifted by ca. 90°, for clarification of the overall shape.

This technique indicates that aggregates can exist in the different H<sub>2</sub>O/DMSO mixtures of the solvents, both at 10 and 100  $\mu$ M. At the latter concentration, a shoulder at 400 nm is always present, regardless of the DMSO content, which is also consistent with the formation of aggregates. However, no aggregates emission is observed for DMSO percentages above 25% (fig. S20). Additionally, these results show that, for the studied solvent mixtures, the structures present similar shape and comparable sizes, although in water the structures are slightly smaller. As such, the loss in emission of the aggregates at higher DMSO content may be related with (1) different types/conformation of aggregates as previously observed in other AGCs<sup>11</sup>; and (2) lower overall concentration of aggregates, which translates into a weaker AIE effect.

### 3.3. Sensing of Guanosine Nucleotides

#### 3.3.1. Influence of Guanosine nucleotides on the optical properties of **3**

The absorption and emission spectra of **3** in the presence of several Guanosine nucleotides, GMP, GDP and GTP, were tested in buffered aqueous media (pH 7.2-7.4, where the nucleotides are fully deprotonated) at two concentrations: 10  $\mu\text{M}$ , below CAC; and 60  $\mu\text{M}$ , above CAC.

In the case of the least concentrated solutions (10  $\mu\text{M}$ ), for all Guanosine derivatives, the response was similar: negligible changes in the absorption spectra and an emission increase of 20-24% at 383 nm (fig. S21). No aggregates band was observed in any of the samples.

For the concentrated solution of **3** (60  $\mu\text{M}$ ), both the absorption as well as the emission spectra were strongly influenced by the presence of Guanosine derivatives, although to different extents. The specific case of Guanosine 5'-monophosphate (GMP) is shown below (fig. 5).

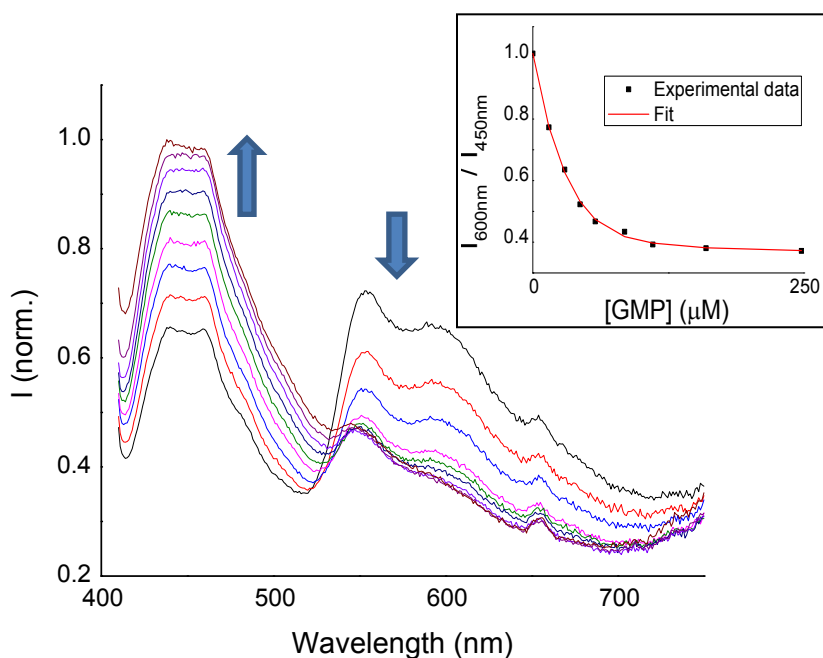


Figure 5. Variation of emission (B,  $\lambda_{\text{exc}} = 400 \text{ nm}$ ) of **3** (60  $\mu\text{M}$  in 10 mM HEPES buffer at pH 7.2) in the presence of Guanosine 5'-monophosphate (GMP). Inset shows the ratio between the emissions at 600 and 450 nm.

For the UV-Vis spectra, an overall decrease in the absorption is observed, including a decrease in the baseline, which may be an indication that some of the higher aggregates are being disrupted (fig. S22).

In the emission spectra, an increase in intensity at 450 nm occurs with increasing concentrations of analyte (this is also observed when exciting the samples at 343 nm, fig. S23). Moreover, a concomitant decrease in the emission band of the aggregates (~600 nm) is observed (fig. 5). This effect becomes weaker as we increase the number of phosphates in the nucleotide, indicating that electrostatic repulsion may play a role on the loss of sensitivity of **3** towards more charged Guanosines (fig. S24).

If we plot the ratio of luminescence between the bands at 600 nm and 450 nm, we obtain a system that behaves as a 1:1 association equilibrium between **3** and the analyte, yielding association constants in the order of  $10^5 \text{ M}^{-1}$  (Table 1), which are, to the best of our knowledge, among the highest recorded for chemosensors based on hydrogen bonding capable of working in aqueous environment (see table S3 for comparison with the literature). Furthermore, the strong signal changes upon analyte binding reach up to 63% variation when compared to the absence thereof, which further highlights the unprecedented sensitivity of this system in aqueous environment.

Table 1. Apparent association constants and percentage in signal change ( $\Delta[\%]$ ) of Guanosine nucleotides with **3** ( $[\mathbf{3}]=60 \mu\text{M}$ ).

Analyte	$K_a (10^5 \text{ M}^{-1})$	$\Delta[\%]$
GMP	1.46	63.3
GDP	4.42	42.0
GTP	1.69	28.7

The values for association constants are within the same order of magnitude for the three studied Guanosine derivatives, being higher for GDP. However, the percentage in signal change ( $\Delta[\%]$ ) varies with increasing number of phosphate groups (GMP > GDP > GTP), which suggests that the negative charges or bulkiness/sterical effects have a significant influence on the overall emission of the aggregates.

### 3.3.2. Computational studies

Naphthyridines have already been reported in the literature as fluorescent units capable of forming stable bonds with guanine derivatives.<sup>11-14</sup> To better understand the specific mode with which our ligand binds to guanine, a series of computational experiments were performed.

We have analyzed two different interaction modes (depicted A and B) by which ligand **2** and Guanine could interact via hydrogen bonding (fig. 6).

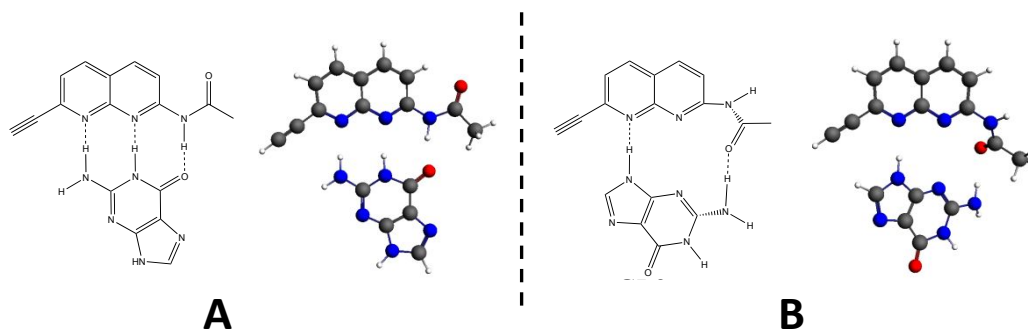


Figure 6. *Ball & stick* representation of two interactions modes, A and B, as possible adducts formed between **2** and Guanine, illustrating the complementarity of hydrogen bonds.

The schematic representation of model A was found to be significantly more stable, since it involves three hydrogen bonding interactions, yielding a complex adduct with nearly perfect planarity, while B comprises only 2 hydrogen bonds (see Table S2, in the Supp. Information). Absorption and emission spectra of **2** in the presence of increasing amounts of Guanine are indicative of this strong interaction, yielding an association constant of  $4.2 \times 10^5 \text{ M}^{-1}$  (fig. S25).

In order to gain further insight on why the association of **3** and phosphorylated Guanosine nucleotides is higher, additional energy calculations were also conducted for the adduct formed from **3** and GMP (fig. 7).



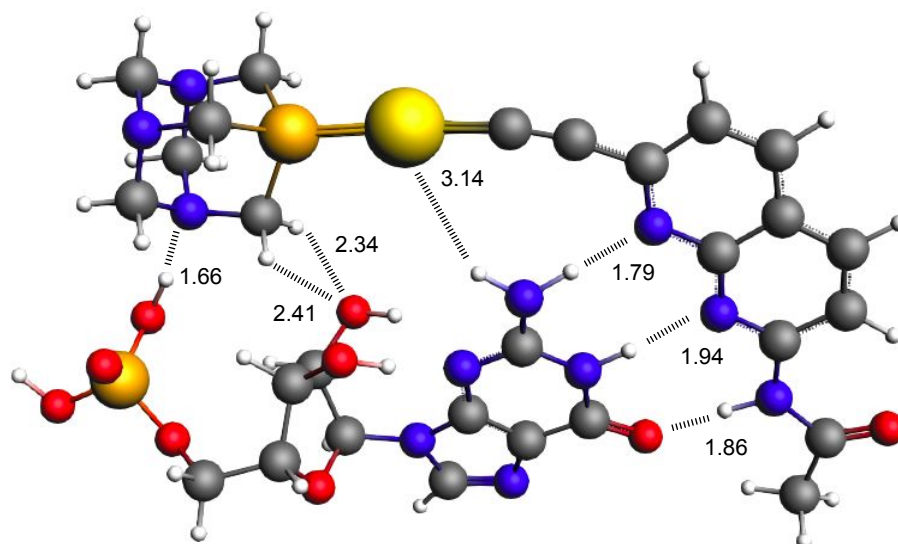


Figure 7. *Ball & stick* representation of the adduct from **3** and GMP. Hydrogen bonding interactions are highlighted, with their respective distances.

Apart from the complementary hydrogen bonds between the naphthyridine ligand and the nucleobase, additional hydrogen bonds are present, between the phosphine ligand and both the sugar and phosphate moieties of the nucleotide. Furthermore, one hydrogen from the guanine nucleobase may also interact with the Au(I) metal center of **3**, given their close proximity ( $\sim 3$  Å). The resulting conformation yields an adduct with a significantly higher stabilization than the adduct formed between **2** and Guanine. The energetic parameter  $\Delta E_{\text{Bond}}$  for all adducts is summarized in table 2.

Table 2.  $\Delta E_{\text{Bond}}$  (kcal/mol) at BLYP-D3/TZ2P in gasphase for all studied adducts.

Adduct	$\Delta E_{\text{Bond}}$
Fig. 6A	-29.9
Fig. 6B	-4.8
Fig. 7 ( <b>3-GMP</b> )	-52.3

#### 4. Conclusions

A new Naphthyridine-ethynyl-Gold(I) complex **3** was synthesized and its structure fully characterized. UV-Vis spectra recorded in water at higher concentrations showed an increase in the baseline, indicating the presence of aggregation. The corresponding emission spectra revealed the appearance of a band with maximum at 550-600 nm, which was absent when the spectra were acquired in a good solvent (DMSO). This Aggregation Induced Emission (AIE) was probably favored by intermolecular (1)  $\pi$ - $\pi$  interactions and (2) aurophilic interactions. Comparison of the emission bands with solid state samples led us to conclude that the AIE band observed in water solutions results from higher aggregates in suspension, since both the position and the lifetimes are essentially the same. Formation of aggregates of around 60 nm diameter was confirmed by SAXS experiments.

Interaction of complex **3** with Guanine derivatives in aqueous media quenched the luminescence of the aggregates while simultaneously increasing the luminescence of free complex, which suggest that the formation of hydrogen bonds with naphthyridine ligand disrupted intermolecular aurophilic bonds, thus diminishing AIE. Apparent association constants and sensitivity (signal variation) were found to be among the highest involving hydrogen bonding sensors in water, to be best of our knowledge. Computational studies comparing adducts formed by the pairs **2/Guanine** and **3/GMP** have further evidenced the strong binding nature of **3** towards phosphorylated Guanosine nucleotides.

The aggregation phenomena of AGCs and their inherent luminescence properties in aqueous environment provide an additional tool for sensing applications based on hydrogen bonding, capable of circumventing the intrinsic competition of water molecules for H-binding sites.

**Conflicts of interest**

There are no conflicts to declare.

## Acknowledgments

This work was supported by the Associate Laboratory for Green Chemistry- LAQV which is financed by national funds from FCT/MCTES (UID/QUI/50006/2019). The authors are also grateful to the Ministry of Economy, Industry and Competitiveness of Spain (AEI/FEDER, UE Projects CTQ2016-76120-P). SAXS experiments were performed at the NCD-BL11 beamline of the ALBA Synchrotron Light Facility in collaboration with the ALBA staff. A.J.M. and J.A. thank FCT for postdoctoral grants (SFRH/BPD/69210/2010 and SFRH/BPD/120599/2016, respectively). The NMR spectrometers are part of The National NMR Facility, supported by FCT/MCTES (RECI/BBB-BQB/0230/2012).

## References

---

1. L. Rodríguez, M. Ferrer, R. Crehuet, J. Anglada, J. C. Lima, *Inorg. Chem.*, 2012, **51**, 7636-7641.
2. R. Chico, E. Castillejos, P. Serp, S. Coco, P. Espinet, *Inorg. Chem.*, 2011, **50**, 8654–8662.
3. A. M. Kuchison, M. O. Wolf, B. O. Patrick, *Inorg. Chem.*, 2010, **49**, 8802–8812.
4. J. C. Lima, L. Rodríguez, *Chem. Soc. Rev.*, 2011, **40**, 5442-5456.
5. R. Gavara, J. Llorca, J. C. Lima, L. Rodríguez, *Chem. Commun.*, 2013, **49**, 72-74.
6. T. Steiner, *Angew. Chem. Int. Ed.*, 2002, **41**, 48-76.
7. D. Blasco, J. M. López-de-Luzuriaga, M. Monge, M. E. Olmos, D. Pascual, M. Rodríguez-Castillo, *Inorg. Chem.*, 2018, **57**, 3805-3817
8. J. Mei, N. L. C. Leung, R. T. K. Kwok, J. W. Y. Lam, B. Z. Tang, *Chem. Rev.* 2015, **115**, 11718–11940.
9. A. Pinto, N. Svahn, J. C. Lima, L. Rodríguez, *Dalton Trans.*, 2017, **46**, 11125-11139.
10. E. Aguiló, R. Gavara, C. Baucells, M. Guitart, J. C. Lima, J. Llorca, L. Rodríguez, *Dalton Trans.* 2016, **45**, 7328-7339.
11. R. Gavara, E. Aguiló, C. Fonseca Guerra, L. Rodríguez, J. C. Lima, *Inorg. Chem.*, 2015, **54**, 5195-5203.
12. E. Aguiló, A. J. Moro, R. Gavara, I. Alfonso, Y. Pérez, F. Zaccaria, C. Fonseca Guerra, M. Malfois, C. Baucells, M. Ferrer, J. C. Lima, L. Rodríguez, *Inorg. Chem.*, 2018, **57**, 1017–1028.
13. L. Shao-Hung, S. Srinivasan, F. Jim-Min, *J. Org. Chem.*, 2007, **72**, 117-122.
14. L. Shao-Hung, P. Riping, F. Jim-Min, *Org. Lett.*, 2016, **18**, 1724–1727.
15. P. J. Cywinski, A. J. Moro, T. Ritschel, N. Hildebrandt, H.-G. Löhmansröben, *Anal. Bioanal. Chem.*, 2011, **399**, 1215–1222.
16. P. J. Cywinski, A. J. Moro, H.-G. Löhmansröben, *Biosens. Bioelectron.*, 2014, **52**, 288–292.
17. P. S. Corbin, S. C. Zimmerman, P. A. Thiessen, N. A. Hawryluk, T. J. Murray, *J. Am. Chem. Soc.*, 2001, **123**, 10475-10488.
18. T. C. Huang, H. Toraya, T. N. Blanton, Y. Wu, *J. Appl. Crystallogr.*, 1993, **26**, 180.
19. J. Kieffer, D. Karkoulis, *J. Phys.: Conf. Ser.*, 2013, **425**, 202012.
20. V. Konarev, V. V. Volkov, A. V. Sokolova, M. H. J. Koch, D. Svergun, *D. I. J. Appl. Crystallogr.*, 2003, **36**, 1277-1282.

21. D. I. Svergun, *J. Appl. Crystallogr.*, 1992, **25**, 495-503.
22. D. I. Svergun, *Biophys. J.*, 1999, **76**, 2879-2886.
23. A. Krebs, H. Durchschlag, P. Zipper, *Biophys. J.*, 2004, **87**, 1173-1185.
24. J. M. Forward, Z. Assefa, J. P. Fackler, Jr., *J. Am. Chem. Soc.*, 1995, **117**, 9103-9104.
25. J. Arcau, V. Andermark, E. Aguiló, A. Gandioso, A. Moro, M. Cetina, J. C. Lima, K. Rissanen, I. Ott, L. Rodríguez, *Dalton Trans.*, 2014, **43**, 4426-4436.
26. A. J. Moro, B. Rome, E. Aguiló, J. Arcau, R. Puttreddy, K. Rissanen, J. C. Lima, L. Rodríguez, *Org. Biomol. Chem.*, 2015, **13**, 2026-2033.